Geochemistry Geophysics Geosystems G3
AN ELECTRONIC JOURNAL OF THE EARTH SCIENCES
Published by AGU and the Geochemical Society

Article
Volume 4, Number 9
27 September 2003
8511, doi:10.1029/2003GC000531
ISSN: 1525-2027

Genovesa Submarine Ridge: A manifestation of plume-ridge interaction in the northern Galápagos Islands

Karen S. Harpp
Department of Geology, Colgate University, Hamilton, New York 13346, USA (kharpp@mail.colgate.edu)

Daniel J. Fornari
Geology and Geophysics Department, Woods Hole Oceanographic Institution, Woods Hole, Massachusetts 02543, USA

Dennis J. Geist
Department of Geological Sciences, University of Idaho, Moscow, Idaho 83844, USA

Mark D. Kurz
Marine Chemistry and Geochemistry Department, Woods Hole Oceanographic Institution, Woods Hole, Massachusetts 02543, USA

[1] Despite its circular coastline and calderas, Genovesa Island, located between the central Galapagos Platform and the Galapagos Spreading Center, is crosscut by both eruptive and noneruptive fissures trending NE-SW. The 075° bearing of the fissures parallels that of Genovesa Ridge, a 55 km long volcanic rift zone that is the most prominent submarine rift in the Galapagos and constitutes the majority of the volume of the Genovesa magmatic complex. Genovesa Ridge was the focus of detailed multibeam and side-scan sonar surveys during the Revelle/Drift04 cruise in 2001. The ridge consists of three left stepping en echelon segments; the abundances of lava flows, volcanic terraces, and eruptive cones are all consistent with constructive volcanic processes. The nonlinear arrangement of eruptive vents and the ridge's en echelon structure indicate that it did not form over a single dike. Major and trace element compositions of Genovesa Ridge glasses are modeled by fractional crystallization along the same liquid line of descent as the island lavas, but some of the glasses exhibit higher Mg # than material sampled from the island. Most of the submarine and the subaerial lavas have accumulated plagioclase. Incompatible trace element abundances of dredged Genovesa Ridge rocks are lower than the island's lavas, but ratios of the elements are similar in the two settings, which suggests that the island and ridge lavas are derived from nearly identical mantle sources. Glass inclusions in plagioclase phenocrysts from the ridge are compositionally diverse, with both higher and lower MgO than the matrix glass, indicative of homogenization at shallow levels. The structural and geochemical observations are best reconciled if Genovesa Ridge did not form in response to injection of magma laterally from a hot spot-supplied central volcano, like Kilauea's Puna Ridge. Instead, Genovesa Ridge and its western extension are the result of passive upwelling directed by far-field tectonic stresses that are generated by tension across the 91°W transform. The proximity of the plume causes magmatism in the extensional zones where it would not ordinarily occur.

Components: 13,627 words, 11 figures, 4 tables.

Keywords: rift zone; seamount; submarine lava flow; mantle plume; plume-ridge interaction; helium.

Index Terms: 3045 Marine Geology and Geophysics: Seafloor morphology and bottom photography; 8429 Volcanology: Lava rheology and morphology; 3640 Mineralogy and Petrology: Igneous petrology.

Received 24 February 2003; **Revised** 8 July 2003; **Accepted** 28 July 2003; **Published** 27 September 2003.

Harpp, K. S., D. J. Fornari, D. J. Geist, M. D. Kurz, Genovesa Submarine Ridge: A manifestation of plume-ridge interaction in the northern Galápagos Islands, *Geochem. Geophys. Geosyst.*, *4*(9), 8511, doi:10.1029/2003GC000531, 2003.

Theme: Plume-Ridge Interacton **Guest Editor:** David Graham

1. Introduction

[2] The northern subprovince of the Galápagos Archipelago is a 100–200 km wide swath bounded by the main Galápagos Platform to the south and the Galapagos Spreading Center (GSC) to the north (Figures 1 and 2). This area is one of the few on the globe subject to the simultaneous influence of both plume and ridge related mantle processes without being dominated by either phenomenon. In the past ~10 My, the plume-ridge system has evolved from a ridge-centered hot spot to its current configuration, with the GSC located 100–200 km north of the hot spot center (Figure 1) [*Wilson and Hey*, 1995]. Studies of submarine lavas erupted along the GSC have provided geochemical evidence for extensive plume-ridge interaction [e.g., *Verma and Schilling*, 1982; *Verma et al.*, 1983; *Schilling et al.*, 1982; *Detrick et al.*, 2002]. Subaerial and submarine lavas from the Galápagos Archipelago indicate that the plume is in turn strongly influenced by the GSC, resulting in a heterogeneous distribution of plume material in the upper mantle throughout the region [e.g., *Geist et al.*, 1988; *White et al.*, 1993; *Kurz and Geist*, 1999; *Harpp and White*, 2001].

[3] The GSC is currently migrating to the northeast at ~50 km/my, away from the hot spot [*Wilson and Hey*, 1995; *Gripp and Gordon*, 1990, 2002]. The large transform fault at 91°W began to form at ~2.6 Ma [*Wilson and Hey*, 1995]. Since that time, the ridge segment closest to the archipelago has undergone several southward jumps [*Wilson and Hey*, 1995], prolonging the proximity of the ridge to the plume [e.g., *Small*, 1995].

[4] The islands and seamounts of the northern Galapagos Archipelago do not lie downstream in terms of absolute plate motion from the hot spot center (thought to be in the vicinity of Fernandina Island [e.g., *Toomey et al.*, 2001; *Kurz and Geist*, 1999] (Figure 1) and consequently cannot be the products of plume activity in the traditional sense. Furthermore, the complex seafloor morphology [*Christie and Fox*, 1990], wide range of geochemical compositions [e.g., *Harpp and White*, 2001], and lack of systematic alignments of seafloor or island features with absolute or relative plate motion [e.g., *Harpp and Geist*, 2002] (Figure 1) suggest that the northern Galápagos volcanoes are not conventional near-ridge seamounts either. Instead, processes resulting from the far-field tectonic interaction between the plume and the ridge are the primary factors controlling the style and distribution of volcanic activity in the northern Galápagos [*Harpp et al.*, 2002; *Harpp and Geist*, 2002]. A detailed examination of volcanic structures in the region between the Galápagos plume and ridge has the potential to reveal important information about plume-ridge interaction and the dynamics of ridge migration processes near plumes.

[5] During the 2001 DRIFT04 expedition on R/V Revelle, we performed multibeam bathymetric mapping and side-scan sonar surveys using the University of Hawaii's Mapping Research-1 (MR-1) system along an east-west profile extending from ~50 km east of Genovesa Island to the northern tip of Isabela Island. The focus of this survey was the 50 km-long ridge that extends east of Genovesa Island [*Harpp et al.*, 2002] (Figures 2 and 3), hereafter referred to as the Genovesa Ridge.

[6] Seafloor imagery revealed that several aspects of Genovesa Ridge are enigmatic. The 075° trend of the ridge is oblique to both the absolute plate motion (91°) [*Gripp and Gordon*, 1990] and plate spreading relative to the GSC (~189°) [*DeMets et al.*, 1994]. The submarine ridge is aligned with a series of large fissures that cross-cut other structural features of Genovesa Island and that produced the volcano's youngest subaerial flows [*Harpp et al.*, 2002] (Figure 3). West of Genovesa

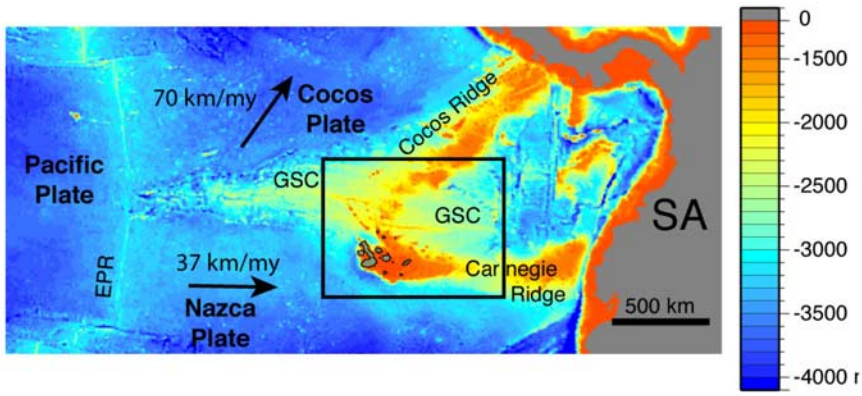

Figure 1. Bathymetric map of the northern Galapagos Archipelago (adapted from *Smith and Sandwell* [1997]). Plate motion vectors for the Nazca and Cocos Plates are from *Gripp and Gordon* [1990].

Island, another submarine ridge extends toward Marchena Island, where it bends NW toward Pinta Island.

[7] Volcanic submarine ridges throughout the study area differ from those observed in Hawaii, such as the submarine part of Kilauea's East Rift Zone, Puna Ridge [e.g., *Fornari et al.*, 1978; *Lonsdale*, 1989; *Smith et al.*, 2002]. On the basis of morphometric and geochemical data, we propose that Genovesa Ridge and its western extension are the result of passive upwelling directed by far-field tectonic stresses that arise from plume-ridge dynamics, instead of active supply by laterally injected magma from a hot spot-supplied central volcano, like Kilauea's Puna Ridge. Our results further suggest that the seamounts, ridges, and islands in the Northern Galapagos region serve as indicators of paleostress fields caused by recent plume-ridge interactions.

2. Shipboard Data Collection

[8] The MR-1 side scan sonar system is an 11/12 kHz near-surface towed sonar system capable of ensonifying large areas of seafloor and collecting coregistered backscatter and phase-bathymetric data [*Rongstadt*, 1992; *Davis et al.*, 1993]. Typically, the width of the side-scan imagery, as controlled by the second multiple return ($\sim$72° from the vertical) is $\sim$5 times the water depth in the deeper parts of the survey area and can be as wide as $\sim$8$\times$ in depths shallower than $\sim$1000 m (M. Edwards, personal communication 2002). Because R/V *Revelle* is equipped with a Simrad EM-120 multibeam sonar, we used only multibeam sonar in compiling the bathymetric maps. MR-1 was operated using an external trigger to synchronize the transmit cycle with the Revelle's EM-120 multibeam sonar. Attempts were made to optimize EM-120 cycle to allow greatest possible side scan return. MR-1 pulse width was adjusted based on water depth and EM-120 cycle and varied between 2 ms for water depths <1000 m to 10 ms for depths >3000 m. This resulted in EM120 system cycles of between 6 and 20 s. MR-1 was used at full power for all surveying.

[9] The simultaneous collection of MR-1 side scan sonar data and multibeam data during the DRIFT04 cruise allowed near real-time production of detailed side-scan backscatter and bathymetry maps. Bathymetric data were gridded at 100 m and side-scan data were gridded at 8 m spacing. This permitted shipboard identification of zones of volcanic construction and contact relationships between structural and volcanic features, as well as areas of inferred recent activity (e.g., highly reflective, sparsely sedimented, young lava flows). The maps were used to identify sample collection sites, in an attempt to characterize the various seafloor features.

[10] The primary mapping and sampling were conducted around Fernandina and southern and northern Isabela Island [*Fornari et al.*, 2001; *Kurz et al.*, 2001]. The mapping conducted northeast and west of Genovesa Island covers an area of >2,200 km^2

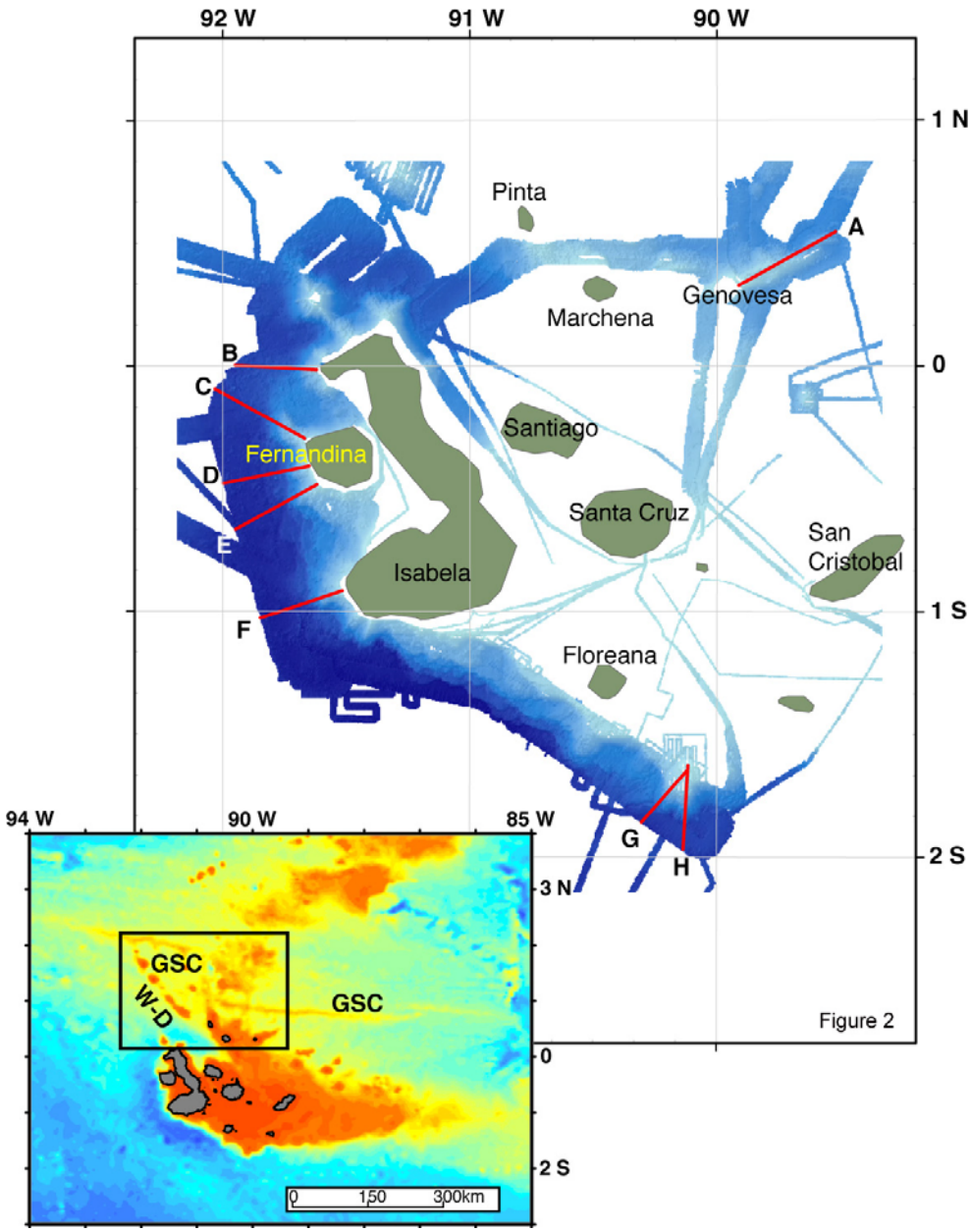

Figure 2. Overview of the study area from the Revelle/Drift04 cruise (2001). Red lines indicate locations of rift zone profiles shown in Figure 6. Inset: Map of Galapagos Archipelago region; black box indicates northern Galapagos subprovince; W-D, Wolf-Darwin Lineament; GSC, Galapagos Spreading Center.

and provided an opportunity for comparison with submarine volcanic rift zones observed off western Fernandina and to the north and south of Isabela, as well as other prominent, well-studied oceanic island rift zones (e.g., Puna Ridge, Hawaii). The processed and mosaiced side-scan and multibeam bathymetry for Genovesa Ridge are presented in Figures 3–5.

[11] Dredging was carried out using the 9/16″ steel trawl wire and standard SIO dredges with a weak-link system. Dredges were lined with netting and a burlap inner-bag was attached to the bottom of the net bag to aid in catching smaller samples and glass shards. A 12 kHz pinger was used for all dredging to establish accurate length of wire scope on the bottom. The pinger was placed at 200 m above the

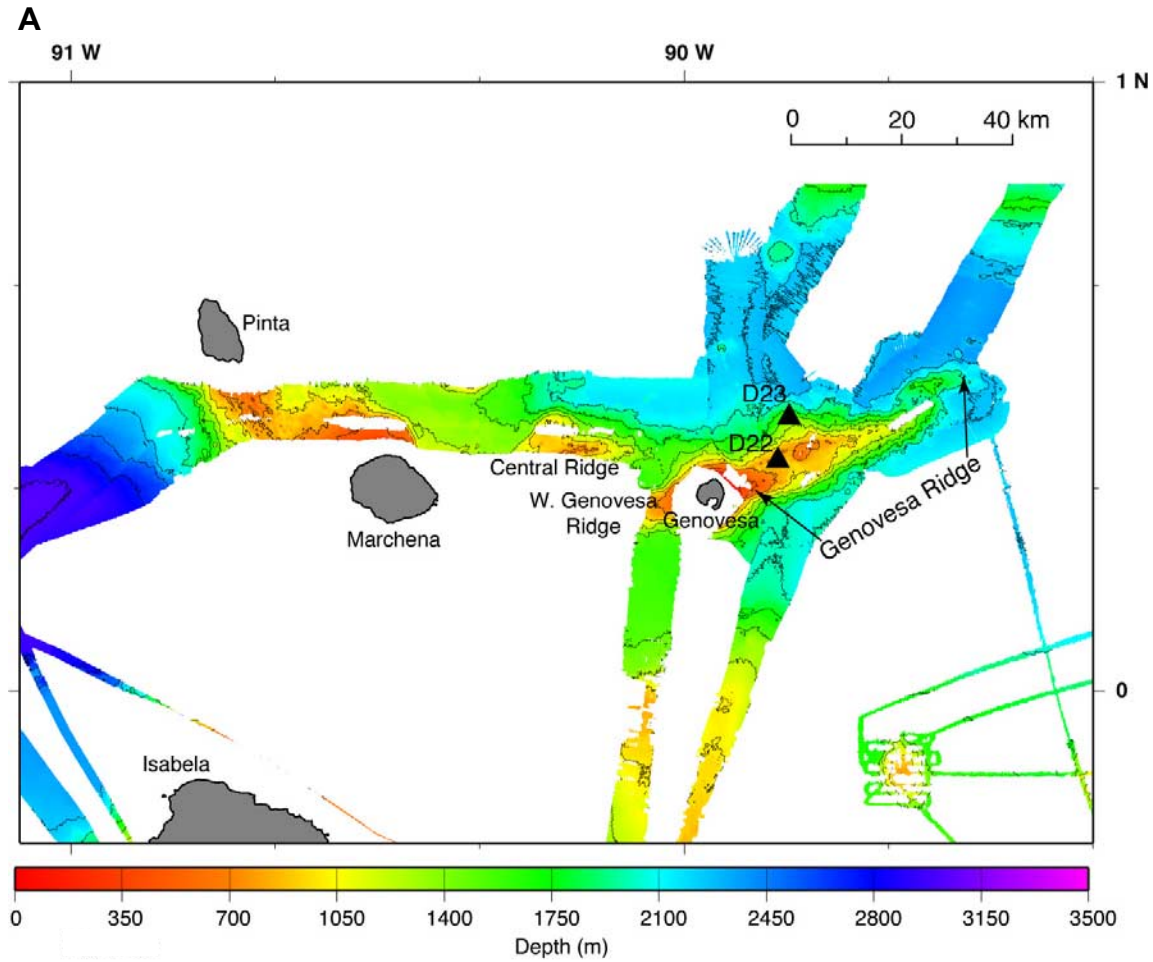

Figure 3. Overview of Genovesa Ridge region. (a) EM120 multibeam bathymetric data. (b) MR-1 side-scan sonar data (G: Genovesa Island, P: Pinta Island; M: Marchena Island). White areas in backscatter images have low sonar reflectivity or are in acoustic shadow, while dark regions represent high-reflectivity areas and steep slopes. Dredge locations are indicated by triangles. Regional contours are from ETOPO2, accessible at http://www.ngdc.noaa.gov/mgg/fliers/01mgg04.html.

dredge for all sampling operations. Main weak links were set between ~18k–21k with side links set a 7.5k each. A weight was placed in a burlap bag for each dredge and tied into the bottom of the dredge bag to collect glass shards and to minimize the possibility that the dredge bag would foul the mouth of the dredge. The bag surrounding this weight was replaced on every dredge to avoid contamination. Dredges were run at a ship's speed over ground of ~1/2 knot using Dynamic Positioning.

[12] Two dredges were successful along the Genovesa Ridge, one at the crest of segment B at the base of a large cone (D22) and the other at the base of the northern ridge flank (D23; Figures 3–5).

3. Sonar Data Analysis

3.1. Bathymetry

[13] Genovesa Ridge extends ~55 km northeastward from the flanks of Genovesa Island. The ridge consists of a series of three left stepping, en echelon segments that vary in length from 12 to over 30 km and are offset by ~2 km (segments A, B, and C, Figures 3–5). West of Genovesa Island, a fourth en echelon segment (Central Ridge) is

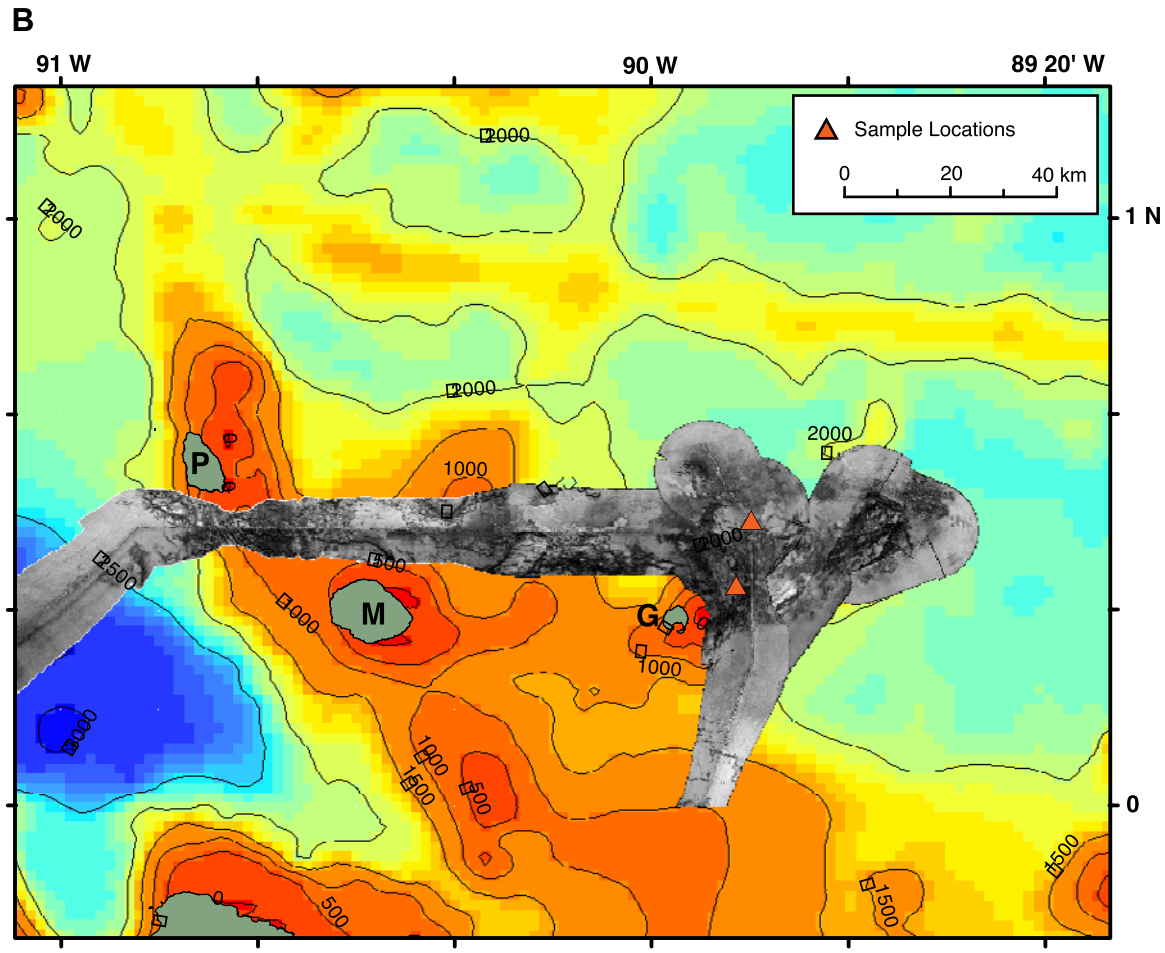

Figure 3. (continued)

offset more than 4 km in a right step sense, but current bathymetric coverage is insufficient to describe this structure in detail (Figure 3).

[14] Segment C forms the northeast tip of the ridge and is the smallest, deepest segment. It trends 088°, is ~13 km long, and overlaps segment B by nearly 5 km. Segment B is 31 km long and has many cones on its crest. Segment A is 12 km long and mostly covered by lava flows that cascaded off Genovesa Island. Segments A and B both trend 075°, overlap by ~5 km, and are offset by a 3.5 km left step. At both of the offsets, the three segments of Genovesa Ridge curve toward their nearest neighbor segment (Figures 4 and 5), a characteristic typical of en echelon fractures [e.g., *Thomas and Pollard*, 1993; *Pollard and Aydin*, 1984].

[15] The basal width of Genovesa Ridge ranges from 30 km for the segment supporting Genovesa Island to an average of about 10 km. The crest of the ridge is up to 6 km wide in segment B (Figure 4). The average axial slopes of the segments (discounting volcanic vents) are considerably steeper than the mean slope of the entire ridge, which is ~43 m/km (Figure 6 and Table 1). Segments B and C exhibit convex-up axial profiles with multiple cones along their crests. Segment A has concave-up slopes because of the broad plateau at its crest and fewer flanking cones.

[16] In general, Genovesa Ridge is bounded on its sides by steep flanks that drop precipitously from a nearly flat crest, particularly in the wider parts of the ridge (segments A and B; Figure 4). Genovesa Ridge is similar to other submarine volcanic ridges (e.g., Puna, Walvis, and Ninetyeast ridges [*Angevine et al.*, 1984]) in that its cross-sectional profiles steepen toward the base. Slopes are generally greater on the southern flank (360–690 m/km),

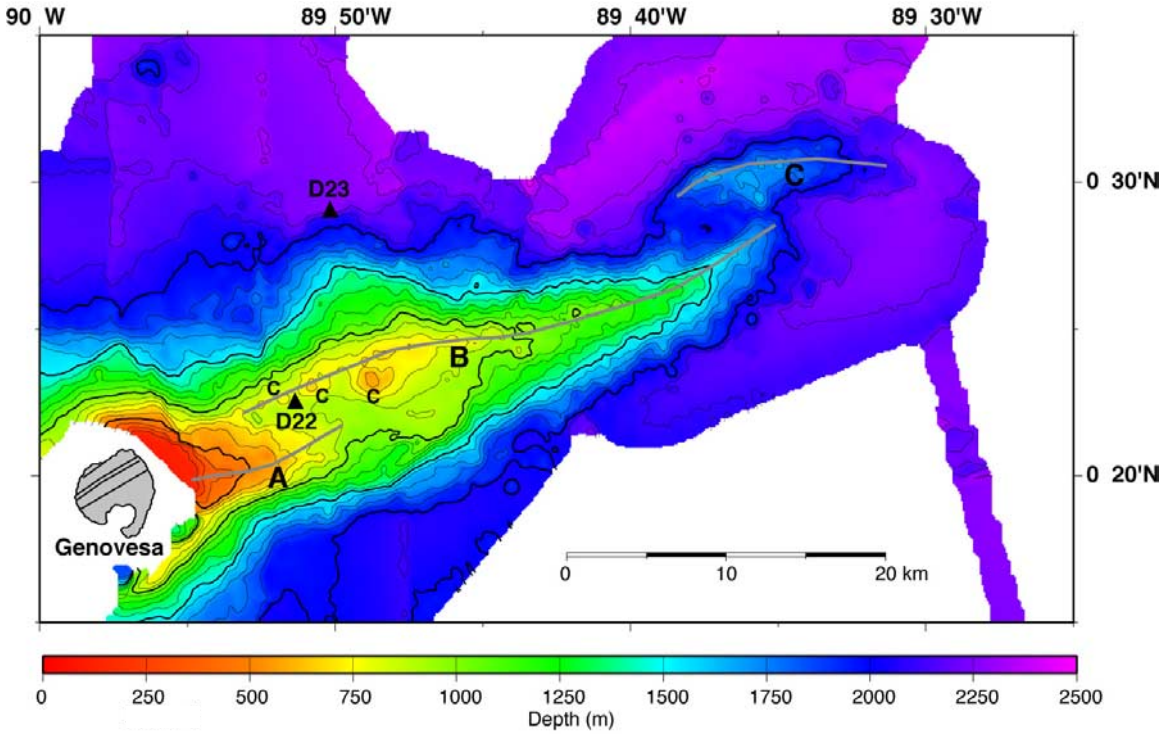

Figure 4. Bathymetry of Genovesa Ridge. Gray lines mark the crests of the en echelon ridge segments A, B, and C, which are labeled with black capital letters. Smaller, black letter "**C**"s are located adjacent to each of the three most prominent crestal cones of segment B. Black lines across Genovesa Island represent the fissures that crosscut the island [*Harpp et al.*, 2002] (see text for explanation). Contour interval is 100 m.

where the gradient abruptly flattens at 2000–2100 m water depth. The northern flank is on average more gently sloping (270–435 m/km), and the wider segments of the ridge (A and B) have small terraces below ~1500 m depth, accounting for the lower overall gradients.

[17] West of Genovesa Island, the submarine ridge continues for ~10 km from the shoreline and may extend ~5 km further ("West Genovesa Ridge"; Figure 3). West Genovesa Ridge (WGR) is morphologically similar to segment A of Genovesa Ridge and has a broad crestal plateau and concave-up flanks; this segment may simply be a westward extension of segment A.

[18] Northwest of WGR and Genovesa Island, the much larger submarine Central Ridge trends 088° and has a summit depth of ~700 m (Figure 3). This structure has a similar volume and elevation to segment B and has a right stepping offset of over 7 km relative to WGR, considerably greater than the en echelon offsets observed east of the island. The lack of complete bathymetric coverage precludes establishing the precise relationship between the Central Ridge and the platform near Marchena and Pinta Islands to its west.

[19] The bathymetry swath between Pinta and Marchena Islands indicates that a broad, ~30 km wide, NW-SE trending submarine platform connects them. North of Marchena, the platform extends ~7 km from the shoreline to the 800 m isobath before the slope steepens abruptly to ~1300 m depth. The western part of the Marchena-Pinta platform has a number of NW-SE structural lineations that are observed in both the bathymetry and side-scan images, which align with the subaerial fissures on Pinta Island [e.g., *Cullen and McBirney*, 1987] (Figure 3). On the northeast part of the platform, several elongate bathymetric highs reach >3 km in length, parallel to the NW-SE strike of the platform as well as the structural trends on Pinta Island [*Cullen and McBirney*, 1987]. The minimum depth of ~500 m in this area occurs on what may be the distal end of a rift zone ridge that extends from Pinta's southern cape, but

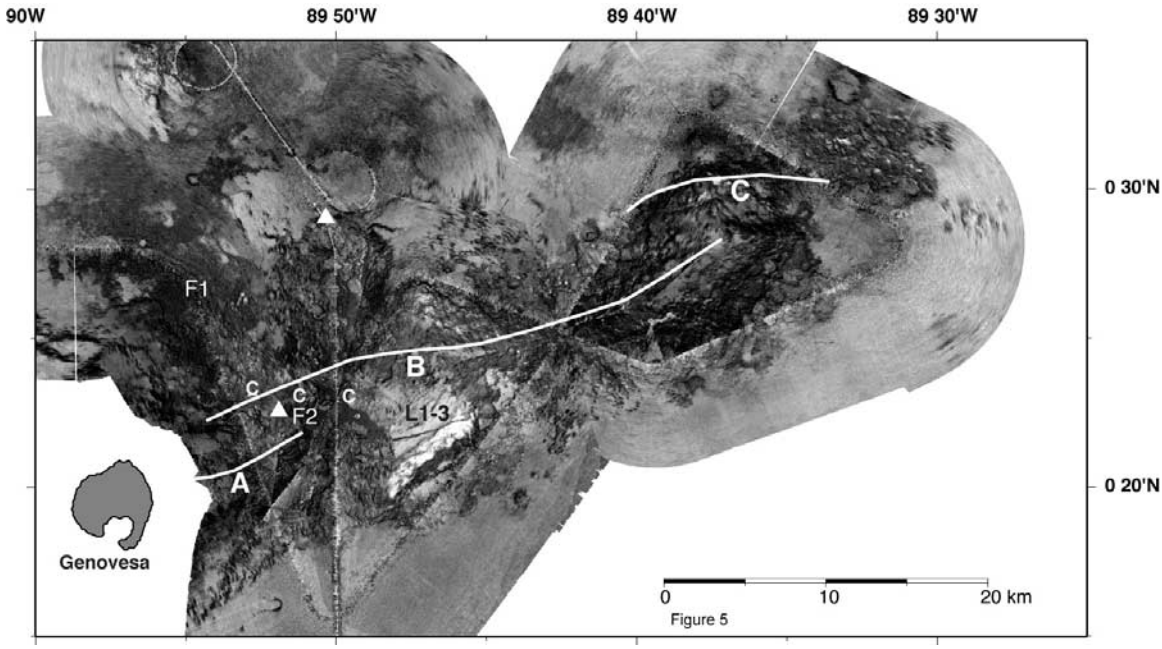

Figure 5. MR-1 side-scan sonar image of Genovesa Ridge. White areas in backscatter images have low sonar reflectivity or are in acoustic shadow, while dark regions represent high-reflectivity areas and steep slopes. Gray lines mark the crests of the en echelon ridge segments A, B, and C. F1 and F2 refer to the large flow fields discussed in the text; labels are located within the flow fields themselves. Flow field F2 bifurcates and cascades both to the north and south between the large crestal cones of segment B, whereas F1 extends northward down the slope of the island onto the adjacent seafloor plain and extends for nearly 19 km. L1, L2, and L3 are lineations discussed in the text and are located beneath and south of their label. White letter "**C**"s are located adjacent to each of the three most prominent crestal cones of segment B.

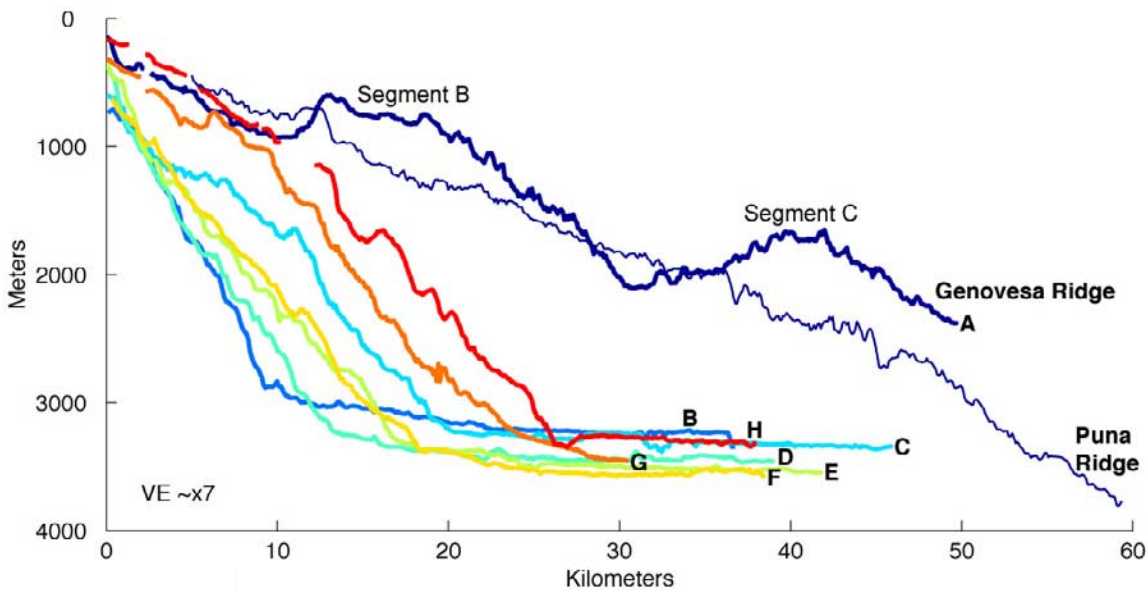

Figure 6. Axial profiles of Genovesa Ridge (A), Kilauea's Puna Ridge, and other Galapagos Archipelago ridges (see Figure 2 for locations of profiles). The valleys in the Genovesa Ridge profile correspond to the regions of overlap between segments A, B, and C.

Table 1. Comparison of Genovesa, Puna, and Fernandina Ridge Characteristics

	Genovesa Ridge	Puna Ridge	Fernandina NW Rift
Length	~50 km (longer if include WGR)	75 km[a]	12.7 km
Width	20 km at widest point ~10 km in most places	>40 km[b]	8 km
Overall trend	075°	065°[a]	Main ridge 310° (curves to N)
Height from seafloor	<2000 m relief	>4000 m relief[a]	>3000 m relief
Overall gradient along axis	43 m/km No continuous crestline slope for length of ridge due to en echelon structure; highly variable slopes.	73 m/km[a] Even crestline[c]	161 m/km (enhanced by location at leading edge of platform); even crestline
Depth at which along axis gradient increases	1000 m (~2/3 along ridge from island)	2700 m[a](~2/3 along ridge from island)	1700 m (~2/3 along ridge from island)
Flank slopes	270–693 m/km	160–275 m/km[d, e]	282–1245 m/km
Offsets along ridge	Between segments A, B, C, and D; left stepping offsets of 2 km for A-B and 1.5 km for B-C; left stepping offset of 4.5 km for C-D.	1 km right stepping offset at ~2700 m depth[a]	Linear to 11 km, then bends to N for remaining 1.7 km; no apparent offset
Volcanic cones	Up to 250 m high, aligned along ridge crest of segments A and B; significantly fewer on C. Cones on flanks are larger and flatter than axial cones.	Up to ~140 m high	None detectable at current resolution.
Pit craters/grabens	No apparent axial graben or significant pit craters.	Many pit craters, often >25 m deep, along crest[c]; nearly continuous graben structures along crest[a]	None detectable at current resolution.
Volumetric relationship of ridge to island	Island is part of one segment; comparable to ridge in volume.	Island is volumetrically dominant relative to ridge	Island is volumetrically dominant relative to ridge.

[a] *Smith et al.* [2002].
[b] *Clague et al.* [1994] (Puna Ridge map USGS).
[c] *Lonsdale* [1989].
[d] *Smith and Cann* [1999].
[e] *Fornari et al.* [1978].

nearshore bathymetry coverage is missing. Along the SW edge of the platform and below 2000 m depth, the gradient decreases sharply where it meets what may be a series of large terraces similar to those observed south and west of Isabela Island [*Fornari et al.*, 2001; *Kurz et al.*, 2001].

3.2. Side-Scan Sonar and Description of Volcanic Features

[20] MR-1 side-scan sonar imagery from the Genovesa Ridge area is characterized by a wide range in reflectivities, as well as textural complexities (Figures 3b and 5), including (1) acoustically smooth, sediment-covered areas north and south of Genovesa Ridge, as well as SW and east of the Marchena-Pinta platform; (2) mottled (patchy, high and low) backscatter areas; and (3) regions of high backscatter that encompass the steep slopes and crest of the ridge where lava flow fronts and cones are dominant.

3.2.1. Lava Flows

[21] Two broad categories of lava flows are observed along Genovesa Ridge. The first type covers most of the ridge and consists of small, lobate structures with reflectivities that vary over short distances (<10 m), likely indicative of a range in weathering, sediment cover, or flow-top morphology (Figure 5). In general, the lobes are better defined on the north flank than they are to the south, where the steeper slopes may inhibit their formation. The sonar imagery is more difficult to interpret on the south flank, however, because of the overall strong backscatter from the steep slopes. At

the base of the ridge, particularly on the southern flank, the texture of the flows is rougher than higher up on the ridge. The apparent roughness may be the result of talus accumulation at the base of the flank caused by auto-brecciation of flows on steep slopes, similar to those observed on the south submarine flank of Kilauea, Hawaii [e.g., *Holcomb et al.*, 1988].

[22] The second category of lava flow appears to be the youngest material on the ridge and is observed primarily on segments A and B. Those flows are characterized by expansive regions of high reflectivity that extend down the north flanks of the ridge onto the surrounding seafloor (Figure 5). These areas are interpreted as relatively fresh, unsedimented lava flows with pillow to lobate morphology, on the basis of their consistently high backscatter signal, tendril-like plan structure, and tendency to expand in area down slopes. Typical examples of these are flow fields F1 and F2, which cover ~170 km^2 and 29 km^2, respectively (Figure 5). The resolution of the sonar data limits our ability to determine whether these flow fields were produced during single or multiple eruptive events.

[23] Flow fields F1 and F2 appear to originate from large cones on the summit of segment B (Figures 5 and 7). The flows overlie less reflective material and therefore must be younger than the main structures of segments B and C. The existence of these flanking flows indicates that the Genovesa Ridge does not consist exclusively of pillow style lavas and clastic debris, as has been documented at other submarine volcanic rift zones [e.g., *Moore and Fiske*, 1969]. Genovesa Island, Marchena Island, and West Genovesa Ridge are also sources for similar lava flows that are large, widely separated, and flat lying compared to those that blanket the Genovesa Ridge.

[24] West of Marchena, where the ridge trends to the northwest, the highest sonar reflectivities are observed in a region midway between Marchena and Pinta Islands. Despite a relatively gentle slope, the terrain is hummocky and lacks the well-defined flow-lobe structures observed along the Genovesa Ridge. We interpret this area of high reflectivity between Marchena and Pinta as some of the youngest lavas in the study area. It is also possible that the shallow saddle area between the islands serves to funnel strong bottom currents through this region, thereby keeping it free from significant sediment accumulation.

3.2.2. Submarine Terraces

[25] In a detailed morphological study of the Puna Ridge, Hawaii, *Smith et al.* [2002] define the submarine terraces imaged by multibeam sonar and 120 kHz side-scan sonar as flat features that are nearly circular in plan, with virtually no relief on their upslope side. The dimensions of the Puna Ridge terraces are up to a few kilometers in width and several hundreds of meters high, and they are often found as a sequence of overlapping steps. Some have flat or mildly inflated surfaces, whereas others may possess summit craters and are thought to be tube-fed structures.

[26] Genovesa Ridge has similar but smaller terrace features, particularly along the ridge crest. These terraces are up to 2 km across and 100 m high. At the tips of the segments, many exhibit domed structures (~25 m high). Some of the terraces are adorned with rows of cones (e.g., east crest of segment B), comparable to structures *Smith et al.* [2002] have interpreted as secondary "rootless" vents above lava tubes that constructed the terraces.

[27] The flows that originate from subaerial vents on Genovesa and Marchena Island, as well as those constructing the northern part of West Genovesa Ridge, form a different type of terrace. Instead, these terraces are far more extensive, up to about 10 km across. They are morphologically similar to the submarine terraces between Fernandina and Cerro Azul volcanoes and south of Isabela and Floreana Islands [*Fornari et al.*, 2001].

3.2.3. Volcanic Cones

[28] Genovesa Ridge bears numerous cones, which are concentrated along crests of the ridge segments and on the lower ridge flanks, below ~1900 m depth. Cones on or near the Genovesa Ridge crest are taller, more pointed, and have smaller basal areas than those on the lower flanks. The crestal

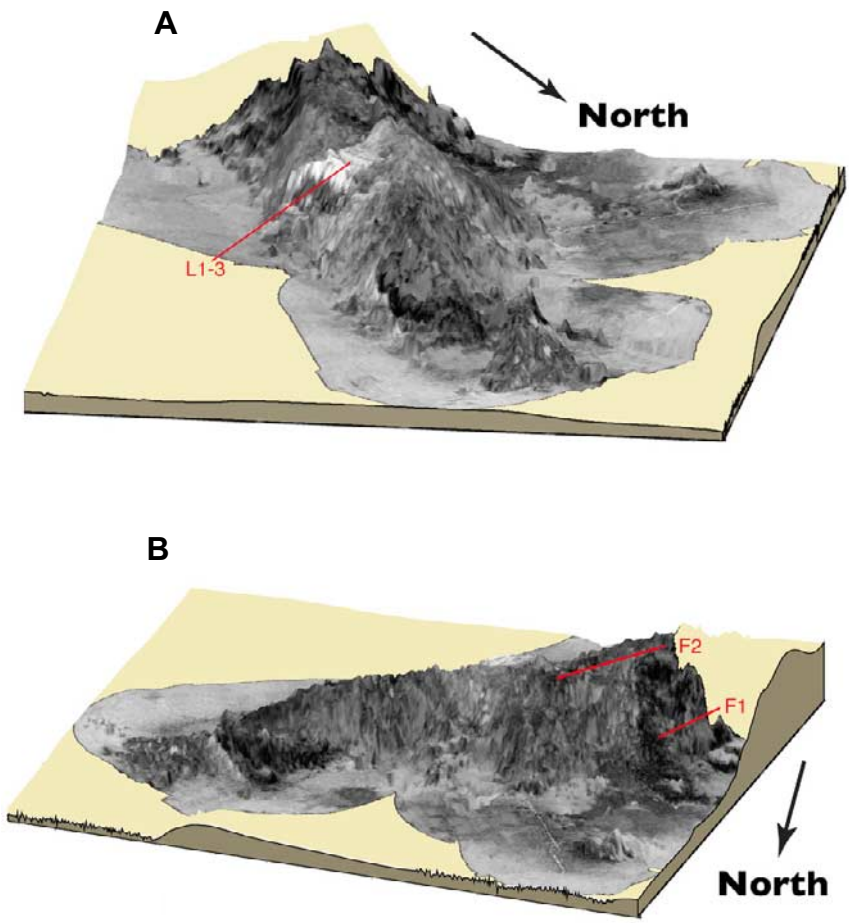

Figure 7. Three-dimensional views of Genovesa Ridge produced by draping the MR-1 side scan sonar data over multibeam bathymetry. The area covered is the same as that shown in Figure 5, approximately 50 km along ridge strike. White areas are low reflectivity and mostly sediment covered, and dark areas are high reflectivity, including areas of high slopes and recent lava flows. Vertical exaggeration is ~5x. (a) View is to the NW up the axis of Genovesa Ridge toward the island with lineaments L1-3 shown. (b) View shows the northern flank of Genovesa Ridge. Flow fields F1 and F2 are the darkest, most highly reflective areas indicated by the red lines; F1 cascades down the north flank of the ridge, and F2 is only just visible at the ridge crest as a region of darker, more highly reflective material.

cones range in height from over 250 m down to ~40 m. Their height to basal diameter ratio is ~6–7%, less than is usual for Pacific basin volcanoes [*Smith and Jordan*, 1988]. Virtually all the cones are aligned along the crest of the ridge. Segment A has fewer cones than the other segments. The axis of segment B is dominated by 3 large cones that achieve water depths shallower than 700 m and appear to have been the sources of one or more of the large, most recent lava fields (F1 and F2; Figures 5 and 7). Most of the cones on Genovesa ridge are nearly equant, without significant elongation along strike of the ridge, unlike the fissure vents of the Puna Ridge [*Smith et al.*, 2002], pillow ridges of the East Pacific Rise [*Fornari et al.*, 1998, unpublished data], or many of the subaerial radial vents on the western Galápagos shields [*Chadwick and Howard*, 1991].

[29] Cones on the ridge flanks and particularly in the deepest areas north of Genovesa Ridge have smaller height to basal diameter ratios (~4–5%), often taking on flat-topped morphologies similar to structures observed near submarine rift zones in Hawaii [e.g., *Clague et al.*, 2000]. Thus, as a generalization, cones become flatter,

Table 2. Major Element Contents of Dredged Lavas[a]

	SiO_2	Al_2O_3	TiO_2	FeO	MnO	CaO	MgO	K_2O	Na_2O	P_2O_5	SO_2	Total
Glasses[b]												
D22-A	48.49	14.93	1.20	9.86	0.18	13.24	8.19	0.05	2.74	0.06	0.12	99.12
D22-B	48.15	15.16	1.17	9.86	0.17	13.24	8.28	0.05	2.67	0.07	0.12	98.94
D22-C	48.48	14.93	1.19	10.00	0.19	13.27	8.08	0.05	2.72	0.09	0.13	99.12
D22-D	47.97	16.37	1.01	8.68	0.16	13.31	9.10	0.06	2.57	0.05	0.27	99.54
D22-E	48.45	14.98	1.19	9.87	0.17	13.27	8.08	0.07	2.78	0.07	0.32	99.25
D22-F	48.66	14.95	1.20	10.08	0.19	13.18	8.01	0.05	2.76	0.08	0.15	99.32
D22-G	48.70	14.91	1.22	10.15	0.19	13.14	7.97	0.06	2.78	0.08	0.15	99.34
D22-H	48.58	15.15	1.20	10.10	0.21	13.46	7.79	0.07	2.74	0.07	0.33	99.69
D22-I	48.74	15.04	1.17	9.90	0.19	13.22	8.27	0.05	2.76	0.08	0.12	99.53
D23-A	49.42	14.72	1.27	10.33	0.18	12.98	7.82	0.06	2.86	0.10	0.14	99.87
D23-B	48.83	14.60	1.24	10.37	0.18	12.92	7.71	0.05	2.82	0.09	0.12	98.93
D23-C	49.13	14.79	1.24	10.36	0.21	12.89	7.87	0.05	2.84	0.08	0.14	99.6
D23-E	49.06	14.66	1.32	10.68	0.20	12.85	7.67	0.06	2.93	0.07	0.15	99.54
D23-F	49.13	14.47	1.31	10.63	0.19	12.78	7.61	0.06	2.96	0.09	0.14	99.41
D23-G	49.37	14.59	1.25	10.49	0.21	12.95	7.89	0.05	2.87	0.06	0.13	99.86
D23-H	49.09	14.51	1.33	10.70	0.20	12.81	7.65	0.06	2.93	0.07	0.14	99.48
D22-D Glass Inclusion 1	49.95	14.42	0.82	8.71	0.18	12.62	9.84	0.07	2.48	0.06	0.21	99.36
D22-D Glass Inclusion 2	50.12	15.15	0.81	8.40	0.15	12.95	9.60	0.06	2.62	0.01	0.23	100.1
D22-D Glass Inclusion 3	50.52	15.96	0.99	7.72	0.13	12.33	8.80	0.05	2.91	0.06	0.18	99.63
D22-D Glass Inclusion 4	49.72	14.91	1.08	8.38	0.14	12.40	9.23	0.07	2.66	0.11	0.24	98.95
D22-D Glass Inclusion 5	48.97	15.62	0.84	9.36	0.23	12.67	9.36	0.06	2.55	0.08	0.24	100.0
D22-D Glass Inclusion 6	48.75	15.32	0.93	9.51	0.18	12.57	9.42	0.09	2.52	0.04	0.27	99.6
D22-D Glass Inclusion 7	49.87	14.97	0.77	9.72	0.19	13.04	9.06	0.08	2.08	0.03	0.32	100.1
D22-D Glass Inclusion 8	49.14	15.84	0.76	9.30	0.11	13.21	8.52	0.08	2.56	0.07	0.28	99.88
Whole rock[c]												
D22-D	49.77	21.16	0.714	6.02	0.116	12.89	6.86	0.04	1.95	0.046		99.56

[a] D22 location: dredge on bottom: 0°22.54′N, 89°51.42′W, 848 m; dredge off bottom: 0°22.48′N, 89°51.80′W, 779 m. D23 location: dredge on bottom: 0°29.20′N, 89°49.90′W, 2257 m; dredge off bottom: 0°28.69′N, 89°49.85′W, 1995 m.
[b] Concentrations determined by microprobe.
[c] Concentrations determined by XRF.

less tall, but more voluminous with increasing water depth.

3.2.4. Structural Lineations

[30] A set of nearly linear seafloor features is observed in the vicinity of 0°22′N latitude and 89°47′W longitude, on the south flank of Genovesa Ridge (Figures 5 and 7). The highly reflective lineations delimit the southern edge of a low backscatter area corresponding to one of the flattest expanses on the Genovesa Ridge. The most prominent and sharpest lineations (L1 and L2; Figures 5 and 7) are subparallel to the strike of the ridge (075°), but are cut by a slightly diffuse lineation (L3) with a more northerly bearing. Lineations L1 and L2 possess less than 25 m in relief, while L3 coincides with a valley that extends to the NE up a cliff face.

[31] The lineations likely result from slope failure similar to unbuttressed landslide collapse observed off oceanic islands like Hawaii [e.g., *Lipman et al.*, 1988, 2000]. The correspondence of L3 with the minor valley is consistent with this hypothesis, as is the generally higher reflectivity of the lineations relative to the surrounding material. If rock has been exposed by downward movement of slump blocks, reflectivity should be high owing to the steep face, fresh rock, and lack of sediment accumulation. Similar lineations on the Central Ridge (Figure 3b) are parallel to each other and define arcuate traces, reminiscent of slump scars; these structures are also located in a large, flat area of low backscatter. In all observed cases, the seafloor at the base of the ridge beneath the lineations exhibits rough, hummocky morphology, consistent with accumulations of slump debris.

[32] The lineations on the platform between Pinta and Marchena Islands do not form at the top of steeply sloped ridge flanks. The lack of associated slump debris and hummocky terrain suggests

Table 3. Trace Element Contents of Dredge Lavas from Genovesa Ridge

	Sc	V	Cr	Co	Ni	Cu	Zn	Ga	Rb	Sr	Y	Zr	Nb	Ba
Glasses														
D22-A	53.2	298	349	49.6	73.6	130	71.4		0.51	105	30.2	67.1	1.04	6.27
D22-B	51.8	290	340	51.7	96.4	130	71.5		0.59	109	29.9	67.6	1.28	7.76
D22-C	57.4	330	380	54.1	79.4	139	79.0		0.56	112	33.1	75.2	1.14	6.96
D22-D														
D22-E	55.6	317	367	52.1	76.6	135	73.9		0.52	108	32.0	71.5	1.11	6.72
D22-F	52.4	294	344	52.3	97.5	130	72.0		0.58	107	29.9	67.4	1.26	7.69
D22-G	49.1	275	321	48.9	91.7	121	66.8		0.53	100	27.7	62.8	1.18	7.27
D22-H	57.2	316	373	52.8	76.6	133	74.4		0.53	109	32.1	72.1	1.11	6.86
D22-I	55.7	309	366	51.5	76.0	133	73.0		0.52	106	31.7	70.7	1.09	6.61
D23-A	54.3	330	215	54.2	68.6	129	84.4		0.72	97.8	32.3	66.6	1.15	6.62
D23-B	53.7	323	215	53.3	69.5	125	77.3		0.52	95.8	31.6	63.7	1.11	7.43
D23-C	53.1	321	209	53.2	65.4	123	75.7		0.51	96.0	31.8	64.8	1.11	6.15
D23-E	57.0	339	223	57.2	89.6	123	88.9		0.82	119	34.9	81.1	1.78	25.0
D23-F	52.6	313	210	50.3	55.8	120	73.5		0.61	97.4	30.6	68.6	1.33	7.23
D23-G	51.2	318	205	51.9	65.9	122	76.9		0.52	98.0	31.8	65.3	1.12	6.35
D23-H	51.5	309	201	50.3	55.2	124	76.2		0.66	102	31.6	71.7	1.39	7.72
Whole rock														
D22-D[a]	27.0	170	346	42.97	142	105	39.0	15.0	0.34	119	18.0	44.0	1.5	5.99
W-2[b]	36.5	271	91.7	44.9	72.4	105	75.5		20.0	196	22.8	89.8	7.87	168
SD	0.97	9.26	1.94	1.13	2.13	1.93	1.87		0.31	4.54	0.41	1.60	0.11	3.90
Count	20	20	20	20	20	20	25		25	10	25	25	25	25

	La	Ce	Pr	Nd	Sm	Eu	Gd	Tb	Dy	Ho	Er	Tm	Yb	Lu	Hf	Ta	Pb	Th	U
Glasses																			
D22-A	1.72	6.24	1.26	7.32	2.88	1.10	3.89	0.73	4.80	1.07	3.05	0.45	2.82	0.42	1.83	0.07	0.26	0.07	0.01
D22-B	1.86	6.52	1.28	7.31	2.83	1.08	3.80	0.72	4.76	1.05	3.04	0.45	2.80	0.42	1.83	0.08	0.28	0.08	0.02
D22-C	1.87	6.81	1.37	7.97	3.13	1.18	4.20	0.79	5.27	1.17	3.35	0.50	3.10	0.47	2.01	0.08	0.30	0.07	0.01
D22-D																			
D22-E	1.84	6.67	1.34	7.77	3.06	1.17	4.16	0.78	5.15	1.14	3.28	0.48	3.02	0.45	1.95	0.07	0.34	0.07	0.01
D22-F	1.86	6.50	1.28	7.29	2.81	1.09	3.84	0.72	4.79	1.07	3.06	0.45	2.80	0.42	1.82	0.08	0.27	0.08	0.02
D22-G	1.75	6.08	1.19	6.80	2.64	1.02	3.60	0.68	4.49	1.00	2.85	0.42	2.63	0.39	1.70	0.08	0.23	0.08	0.01
D22-H	1.83	6.64	1.33	7.73	3.03	1.18	4.16	0.79	5.20	1.15	3.30	0.49	3.04	0.46	1.96	0.07	0.26	0.07	0.07
D22-I	1.82	6.59	1.33	7.70	3.04	1.17	4.15	0.78	5.15	1.14	3.27	0.48	3.00	0.45	1.96	0.07	0.29	0.07	0.01
D23-A	1.80	6.21	1.25	7.31	2.96	1.15	4.15	0.79	5.22	1.16	3.32	0.50	3.07	0.46	1.90	0.08	0.38	0.08	0.01
D23-B	1.72	6.03	1.21	7.11	2.87	1.11	4.01	0.77	5.08	1.13	3.25	0.48	2.99	0.44	1.84	0.07	0.25	0.07	0.01
D23-C	1.72	6.07	1.22	7.15	2.86	1.13	4.07	0.78	5.10	1.13	3.25	0.49	3.00	0.45	1.84	0.07	0.24	0.07	0.01
D23-E	3.03	8.68	1.58	8.80	3.33	1.26	4.59	0.87	5.68	1.26	3.62	0.54	3.35	0.50	2.19	0.11	1.97	0.14	0.13
D23-F	1.96	6.66	1.29	7.34	2.89	1.10	3.98	0.76	4.97	1.10	3.15	0.47	2.89	0.43	1.89	0.09	0.26	0.09	0.02
D23-G	1.74	6.15	1.24	7.25	2.95	1.15	4.13	0.79	5.22	1.16	3.32	0.49	3.06	0.46	1.89	0.08	0.24	0.07	0.01
D23-H	2.05	6.95	1.36	7.72	3.02	1.16	4.16	0.78	5.19	1.15	3.28	0.49	3.03	0.45	1.98	0.09	0.27	0.09	0.02
Whole rock																			
D22-D[a]	1.19	3.97	0.78	4.49	1.75	0.74	2.36	0.44	2.91	0.64	1.84	0.27	1.69	0.25	1.12		0.48	0.06	0.02
W-2[b]	10.4	22.7	3.02	12.7	3.31	1.08	3.66	0.62	3.84	0.81	2.26	0.33	2.04	0.30	2.29	0.48	7.65	2.13	0.50
SD	0.22	0.47	0.06	0.26	0.07	0.03	0.08	0.02	0.08	0.02	0.05	0.01	0.04	0.01	0.04	0.01	0.22	0.05	0.02
Count	25	25	25	25	25	25	25	25	25	25	25	25	25	25	25	25	25	20	23

[a] Concentrations of Sc, V, Cr, Ni, Cu, Zn, Ga, Rb, Y, Zr, and Nb in D22-D (whole rock) were determined by XRF. All other elements for D22-D and all glass concentrations were determined by ICP-MS.
[b] W-2 is a USGS standard reference material analyzed as an unknown for quality control.

instead that they are fissure vents or noneruptive fractures.

4. Geochemical Analyses

4.1. Petrography

[33] Dredge 22, taken from ~800 m depth along the crest of segment B of Genovesa Ridge, included two types of pillow lavas. Sample D22-D is a plagioclase-ultraphyric basalt, with 15% plagioclase phenocrysts up to 6 mm long, which is petrographically similar to much of the subaerial lava from Genovesa Island [*Harpp et al.*, 2002]. All other specimens collected from Dredge 22 are sparsely plagioclase-phyric, with <1% plagioclase phenocrysts up to 2 mm in length. Dredge 23 was collected from a small escarpment at the northern base of segment B at a depth of ~2126 m (Figures 3–5). All samples from this dredge are lithologically identical and are aphyric pillow lavas with glassy crusts; the rocks are more altered than those from Dredge 22.

4.2. Analytical Methods

[34] Because almost all dredged lavas are glassy, only sample D22-D was analyzed by XRF for major and trace element abundances; all others were examined by electron microprobe and ICP-MS.

[35] Glass and melt inclusion compositions were determined on the Cameca Camebax electron microprobe at Washington State University. Fresh volcanic glass free of visible alteration was carefully hand picked with the aid of a binocular microscope and doubly rinsed in distilled water. The glass analyses were made with a beam diameter of 15–20 microns, current of 10 nA, and potential of 15 kV. A correction for sodium loss by volatilization was made by monitoring variation in Na counts with time. Reported values represent averages of two analyses each of 3–5 separate glass grains.

[36] Bulk rock analyses were performed by XRF in the Geoanalytical Laboratory at Washington State University (D22-D only [*Johnson et al.*, 1999]). Blind triplicate analyses yielded reproducibility at levels of <1% RSD for the major analytes and <5% for the trace elements (Tables 2 and 3).

[37] Trace elements were determined by ICP-MS at Colgate University. Glass chips were hand picked to avoid visible alteration, then ultrasonicated in purified water repeatedly to remove surficial contamination. Between 0.22 and 0.30 g of each sample were heated in closed Teflon containers for 48 hours with 25 mL of a 3:2 mixture of purified HNO_3 and HF acids. The solutions were evaporated to dryness in a HEPA-filtered laminar flow hood, and subsequently redissolved in 25 mL of 50% purified HNO_3. The solutions were transferred quantitatively to 250 mL LDPE bottles and mixed with purified water to achieve a thousand-fold dilution of the original sample.

[38] Trace element analysis was performed on a Hewlett Packard HP4500 inductively coupled plasma-mass spectrometer (Table 3). Samples were run 4–6 times to yield overall precisions of <2% for all analyte masses on replicate analyses (except for Th). Standard curves for each isotope were constructed using USGS Standard Reference Materials BIR-1, DNC-1, W-2, BHVO-2, and AGV-2, yielding Pearson correlation coefficients consistently >0.998. Instrumental drift was monitored using three internal standard isotopes, ^{115}In, ^{133}Cs, and ^{182}W; raw data for each analyte were corrected to the nearest internal standard mass prior to calculating final solution concentrations [e.g., *Eggins et al.*, 1997].

[39] Helium isotopic measurements were performed in the Isotope Geochemistry Facility at Woods Hole Oceanographic Institution (Table 4). All measurements were obtained by in vacuo crushing of cleaned volcanic glass. The glasses were lightly crushed in stainless steel mortar and pestle, and washed in distilled water, nitric acid, distilled water, and acetone prior to hand picking under binocular microscope and placement into the vacuum crushing apparatus (as described by *Kurz et al.* [1995]).

4.3. Major and Trace Elements

[40] Lavas from Genovesa Ridge dredges have Mg # = 56.0 to 65.1 (Mg # = molar MgO/(MgO +

Table 4. Helium Isotopic Measurements on Genovesa Ridge Glasses[a]

Glasses	^{4}He, μcc/g	^{3}He/^{4}He, R/Ra	1 sigma, R/Ra
D22-A	10.4	8.79	0.06
D22-B	0.21	8.60	0.04
D22-D	1.70	8.28	0.05
D22-E	7.84	8.78	0.05
D22-I	7.52	8.50	0.10
D22-F	0.63	8.95	0.06
Average		8.65	
Standard Deviation		0.24	
D23-A	3.05	8.12	0.04
D23-B	3.02	8.12	0.07
D23-E	0.43	8.19	0.04
D23-F	1.00	8.05	0.04
D23-H	0.99	8.17	0.04
Average		8.13	
Standard Deviation		0.06	

[a] All measurements by in vacuo crushing of glass.

FeO*)) and are largely indistinguishable from normal mid-ocean ridge basalt (MORB [e.g., *Sinton and Detrick*, 1992]), with relatively narrow ranges in major and trace element contents (e.g., TiO_2: 1.01–1.33 wt. %; Na_2O: 2.57–2.96 wt.%; Figure 8 and Table 2). Similarly, Genovesa Ridge samples have consistently depleted, MORB-like incompatible trace element compositions (Figures 9 and 10 and Table 3). They exhibit depleted light rare earth element (REE) signatures with slightly positive heavy REE slopes (i.e., $Sm/Yb_{(n)} > 1$), an indication that they may have been generated at greater average depths than typical MORB [e.g., *Wilson*, 1992]. A similar pattern is observed in all subaerial lavas collected from Genovesa Island [*Harpp et al.*, 2002] (Figure 10).

[41] The whole rock composition of D22-D is significantly richer in Al_2O_3 and SiO_2 and poorer in Na_2O than glass from the same sample. Glass inclusions in plagioclase phenocrysts are compositionally more diverse than glass from the quenched rind, but the average of all the inclusions is close to that of the rind glass for most major elements (Figure 8). Lavas from the base of the ridge (D23) have lower Mg # and higher Na_2O, TiO_2, FeO, and SiO_2 contents than the lavas from D22.

[42] In contrast to the major elements, incompatible trace element (ITE) concentrations from the two dredges are nearly indistinguishable (Figures 9 and 10). In particular, most ratios of incompatible trace elements are identical within analytical error, confirming that D22 and D23 lavas originated from similar mantle sources. Slight differences in some trace element ratios, such as $Sm/Yb_{(n)}$ (Figure 10), indicate that melting conditions may have varied slightly with time or in different places.

[43] The trace element variations observed in Dredge 22 can be explained largely by the effects of the abundant, accumulated plagioclase phenocrysts in D22-D (Figures 9 and 10). Despite the major element homogeneity of D23 glasses, variations of the more incompatible elements are greater in D23 glasses than in D22 (e.g., Ba, Zr, Nb, Rb, Sr). Compared to a detailed compositional study of single Icelandic lava flows [*Slater et al.*, 2001], Dredge 23 glasses exhibit up to twice the variation in light rare earth element and Ba concentrations observed in individual Icelandic flows, but similar or less than half as much variation in other highly incompatible elements (including Rb, Xr, Y, Zr, Nb, Ba, and the heavy REEs).

[44] Helium isotopic ratios of the two Genovesa Ridge dredges are close to the putative normal MORB value of ~8 times atmospheric (Ra; Table 4). The average ^{3}He/^{4}He ratio is 8.65 Ra (±0.24, n = 6) for Dredge 22 and 8.13 Ra (±0.06, n = 5) for Dredge 23. The small difference between the two dredges is greater than analytical error, indicating slight differences in mantle source isotopic compositions. In general, ^{3}He/^{4}He ratios close to MORB and slightly lower are observed in the northern Galapagos archipelago [*Graham et al.*, 1993; *Kurz and Geist*, 1999]. The Genovesa Ridge ratios are higher, however, than the maximum value of 8.07 measured from the GSC [*Detrick et al.*, 2002].

5. Discussion

5.1. Mantle Sources and Relationship Between Genovesa Ridge and Island Lavas

[45] Lavas from Genovesa Island and Genovesa Ridge are among the most distinctive in the Galápagos Archipelago. Most notably, they are impoverished in the incompatible elements (includ-

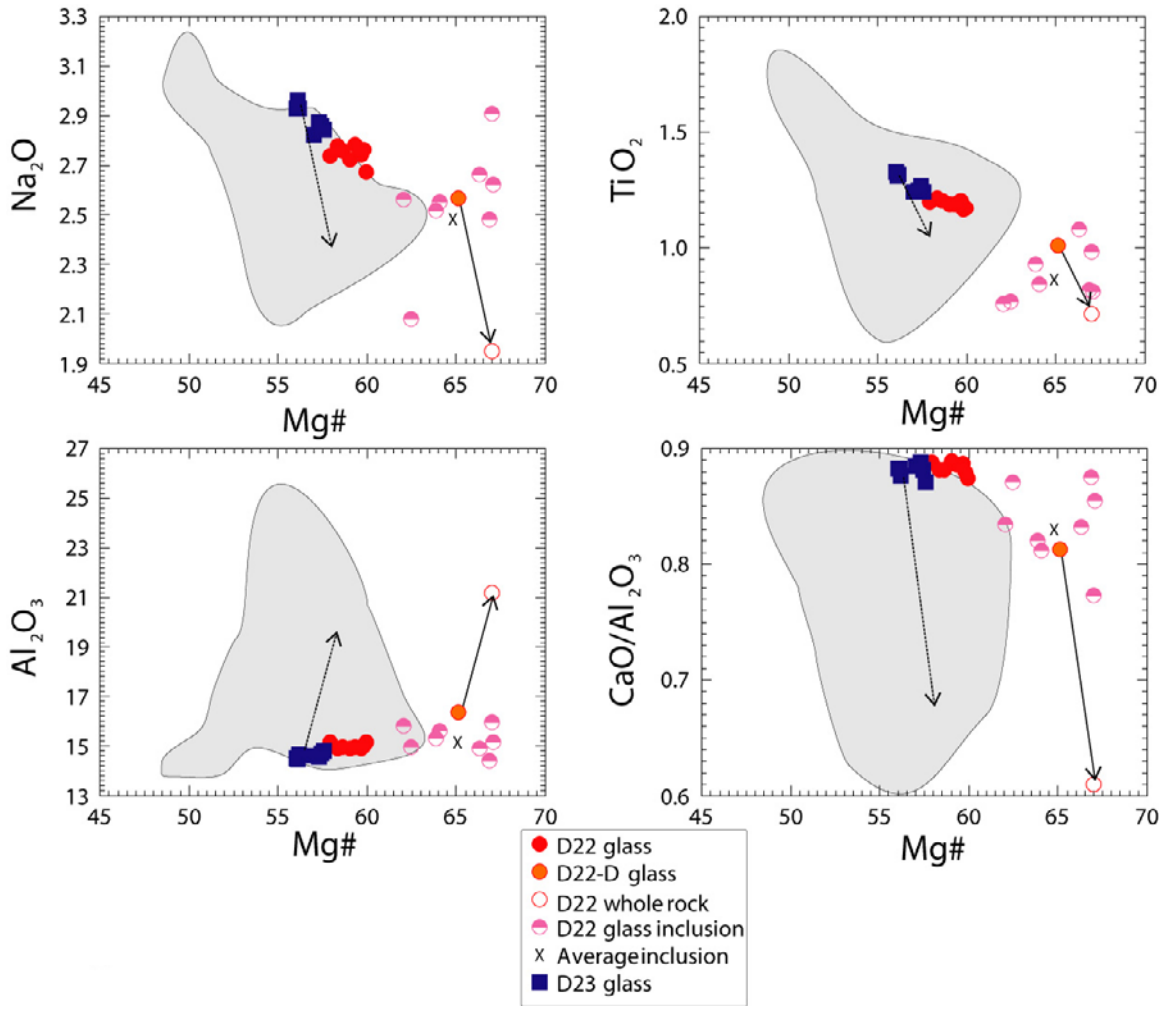

Figure 8. Major element variations in Genovesa Ridge lavas. Comparison of dredged Genovesa glasses (D22 and D23) to subaerial Genovesa Island whole rock analyses from *Harpp et al.* [2002]. Solid arrow connects D22-D glass (tail of arrow) and whole rock (head of arrow) to illustrate the effect of plagioclase phenocryst addition to the melt. The arrow emanating from Mg # = 56 glass also shows hypothetical plagioclase addition.

ing Ti, K, and P), closely resemble normal MORB, and many are ultraporphyritic with large (>1 cm) plagioclase phenocrysts [*Harpp et al.*, 2002]. Therefore the depleted mantle source that feeds Genovesa Island [*Harpp et al.*, 2002] is similar or even identical to that supplying magma to the submarine ridge, and consists primarily of depleted upper mantle.

[46] Most of the differences between the subaerial Genovesa Island and submarine Genovesa Ridge samples can be attributed to variations in the analyzed materials [i.e., glass versus whole rock), the accumulation of plagioclase, and shallow-level fractional crystallization (Figure 8). The compositional differences between the high-MgO porphyritic sample D22-D and the aphyric, lower MgO lavas are likely the result of fractional crystallization of olivine and plagioclase. Increasing Ca/Al ratios with evolution (Figure 8) rules out significant clinopyroxene fractionation, which is important because clinopyroxene is the liquidus phase in these compositions at pressures of greater than ~1 kb (as calculated from the MELTS program [*Ghiorso and Sack*, 1995]). Most fractionation of the Genovesa Ridge magmas therefore must have taken place in the shallow crust, in contrast to magma from the western Galápagos volcanoes, which undergo

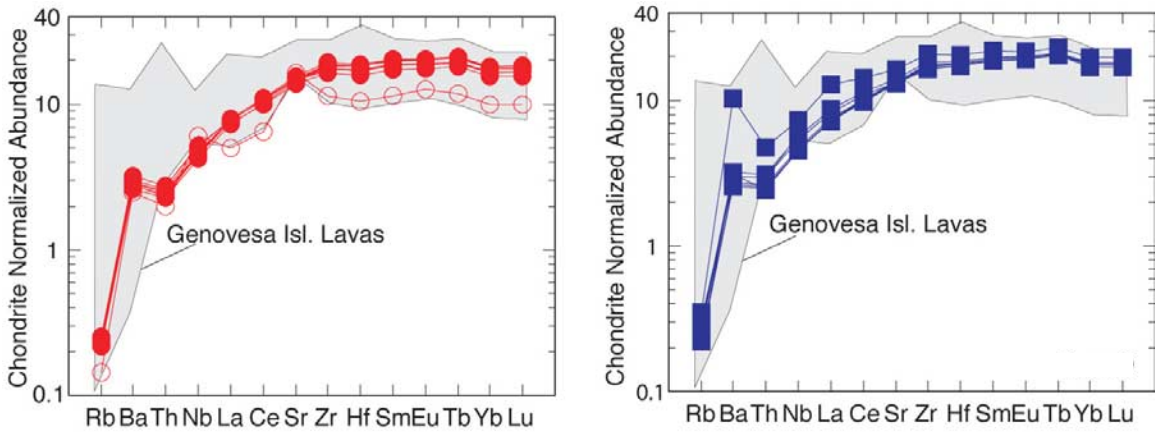

Figure 9. Trace element variations in Genovesa Ridge lavas. (left) Incompatible trace element diagram for Dredge 22 lavas. Chondrite normalization values are from *McDonough and Sun* [1995]. Gray field represents Genovesa Island lavas (whole rock analyses only [*Harpp et al.*, 2002]). (right) Incompatible trace element diagram for Dredge 23 lavas, as in part A.

extensive fractional crystallization in the upper mantle and lower crust [*Geist et al.*, 1998].

[47] Although the major element compositions of lavas from Genovesa Island and Genovesa Ridge are similar and appear to be related primarily by shallow crystallization, subtle differences distinguish the two suites. In terms of major elements, the glass and whole rock major element compositions from sample D22-D are more MgO-rich than any of the subaerial lavas. For some incompatible trace elements and their ratios, the most depleted Genovesa Island lavas and the most enriched submarine-ridge compositions barely overlap (e.g., La_n/Sm_n and Sm_n/Yb_n; Figure 10c). For other ratios (e.g., Hf/Ta, Zr/Nb, La/Ce), the compositions are more distinctive. The incompatible element ratios of most ridge lavas define a trend similar to that exhibited by the island but extending toward more depleted compositions (Figure 10c). Otherwise, the submarine ridge lavas most closely resemble basalts produced during the island's earliest shield-building phase [*Harpp et al.*, 2002].

[48] With the limited set of samples and analytical data, it is not possible to determine whether the island magmas originate from slightly lower extents of melting, or whether they are derived from a slightly less depleted source. The lower $Sm/Yb_{(n)}$ and elevated ITE concentrations (e.g., Rb, Y) of the lavas (Figure 9) from the base of the ridge may be the result of shallower depths and smaller degrees of melting than lavas erupted at the ridge crest [e.g., *Plank and Langmuir*, 1992]. Nevertheless, the higher MgO and more depleted trace element signatures in Genovesa Ridge lavas lead us to believe that the magmatic plumbing systems feeding the ridge and island may not be connected.

[49] The relatively wide compositional range of the glass inclusions in the plagioclase in D22-D suggests that these phenocrysts originated from a number of host magmas, which hybridized and homogenized as the crystals formed. The glass rind composition is similar to the average composition of the inclusions, which supports this hypothesis. The SiO_2 contents of the glass inclusions are problematic, however; all of the inclusions are richer in SiO_2 than are the glass samples (Table 2). This discrepancy is not caused by post-entrapment crystallization. Plagioclase removal would decrease the liquid SiO_2 content, and the crystallization trend is opposite that formed by plagioclase addition (Figure 8). Likewise, the SiO_2 variations in the glass inclusions could not be the result of plagioclase dissolution, as the inclusions are slightly poorer in Al_2O_3 than is the glass (Figure 8). Thus, despite the absence of a discernable relationship between the inclusions and the glass, it is clear that the plagioclase phenocrysts did not simply grow from a liquid with the same composition as the glass [cf. *Cullen*

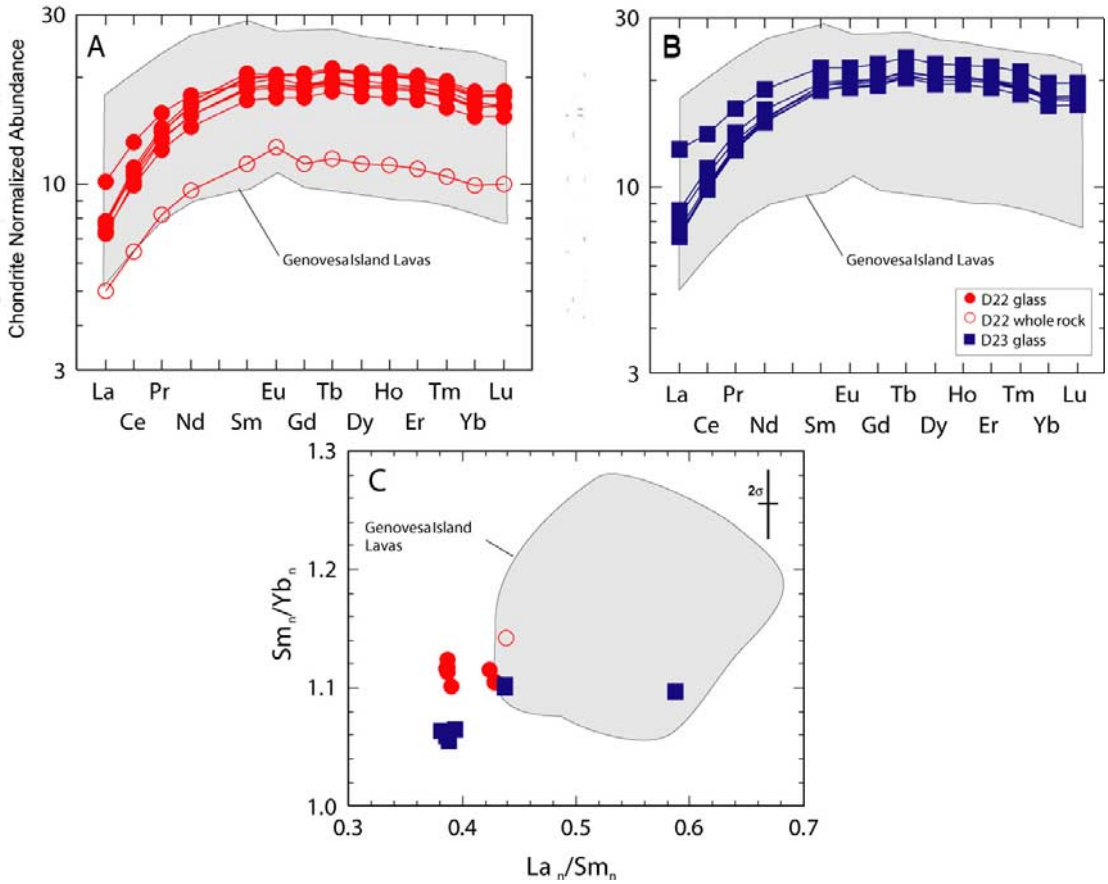

Figure 10. Rare earth element variations in Genovesa Ridge lavas. (a) Rare earth element diagram for Dredge 22 lavas. Chondrite normalization values from *McDonough and Sun* [1995]. Whole rock analyses of Genovesa Island lavas are represented by the gray field [*Harpp et al.*, 2002]. (b) Rare earth element diagram for Dredge 23 lavas, as in Figure 10a. (c) Rare earth element ratios for Genovesa Ridge lavas; gray field is Genovesa Island lavas (whole rock analyses only [*Harpp et al.*, 2002]). Error bars represent 2σ for the calculated ratios, based on analytical error estimates (Table 3).

et al., 1989]. Moreover, the fact that the inclusions exhibit both higher and lower Mg # than the glass indicates that hybridization occurred at shallow levels and between magmas both cooler and hotter than the final erupted magma.

[50] In summary, Genovesa Ridge lavas are derived from depleted mantle sources similar to those of Genovesa Island, have experienced shallow fractionation, and underwent mixing with magmas of variable temperatures prior to eruption. It is possible that the magmas supplying the ridge come from a central, stratified magmatic system beneath the island that intrudes laterally, as has been proposed for the Puna Ridge [e.g., *Clague et al.*, 1995; *Johnson et al.*, 2002]. The compositional distinctions instead suggest that the ridge magmas are fed from a broad melt zone directly underlying the ridge, and that the two systems are not directly connected.

5.2. Evidence of Volcanic Constructional Processes

[51] The morphology of the seafloor in the study area supports the conclusion that the Genovesa Ridge and its extensions toward Marchena and Pinta Islands result from constructional volcanic processes. The abundance of lava flows, volcanic terraces, and eruptive cones provide the most fundamental evidence for this hypothesis. Moreover, the submarine ridges and platforms exhibit

markedly higher reflectivity and rougher surface textures than the surrounding sediment-covered seafloor. The hummocky terrain dotted with cones and prominent terraces is morphologically consistent with sequences of accumulated submarine flows (Figures 3–5).

[52] The boundary between the surrounding seafloor and the submarine ridges is abrupt at the base of the steeply sloping lower flanks of the ridge and is interfingered with young sediment, implying that the volcanic pile has accumulated relatively recently compared to the age of the ocean floor. The basement in this region is ~1.5 Ma [*Wilson and Hey*, 1995] and should be thoroughly sediment-covered, given the high-productivity waters of the archipelago (which is indicated by our regional side scan survey). The distinct lack of sediment cover on the ridges suggests that the constructional volcanism occurred $\ll$1.5 Ma.

[53] Although volcanism is the dominant process for construction of the ridges in the study area, the eruptive activity has been tectonically controlled. The alignment of the cones along the ridge crests, the uniform orientation of flow fronts parallel to the ridge, the elongate structures between Pinta and Marchena that are also parallel to the NW-SE trend of the platform, and the marked orientation of the submarine ridges themselves suggest that the distribution of eruptive material is influenced by stress fields on a regional scale. Furthermore, the systematic shift in ridge orientation from 075° east of Genovesa Island to 088° between Genovesa and Pinta Islands suggests that the direction of the deviatoric stress fields must vary across the northern Galápagos.

5.3. Comparison With the Puna Ridge, Hawaii

[54] At first glance, the Genovesa Ridge appears comparable to other hot spot-related volcanic rift zones such as the Puna Ridge, the submarine extension of the East Rift Zone of Kilauea volcano. The Puna Ridge has been well studied [e.g., *Malahoff and McCoy*, 1967; *Fornari et al.*, 1978; *Holcomb et al.*, 1988; *Lonsdale*, 1989; *Smith et al.*, 2001], most recently by high-resolution morphological analyses using near-bottom side-scan sonar and photoimagery [*Smith et al.*, 2002]. The data for the Genovesa Ridge are far less extensive, having been collected only at the reconnaissance level. As such, it is not possible to compare the fine-scale morphological features of the ridges.

[55] Despite being comparable in size (the Genovesa Ridge is 2/3 the length of the Puna Ridge; Figure 6), and having similarly sharp, steep cross-sectional profiles, additional basic differences between the rift zones suggest they were not formed by the same fundamental mechanisms (Table 1). First, the volume of material erupted on the Puna submarine rift is dwarfed by the volume of the Kilauea structure [*Holcomb*, 1987; *Holcomb et al.*, 1988; *Fornari et al.*, 1978]. In contrast, Genovesa Island is merely the subaerial expression of ridge segment A's peak, and the ratio of the ridge's volume to that of the island is much greater at Genovesa than at the Puna Ridge.

[56] Second, even though Genovesa Ridge lava flow fields have similar volumes to those erupted at the Puna Ridge (Genovesa Ridge flow field F1, assuming ~10 m thickness: >1.5 km^3; Puna Ridge flows: ~2 km^3 each [*Holcomb et al.*, 1988]), the thin, voluminous lava flows of the Puna Ridge are erupted primarily at depths greater than 4500 m [e.g., *Smith et al.*, 2002; *Holcomb et al.*, 1988; *Fornari et al.*, 1978]; on the Genovesa Ridge, many of the large flows originate on or near the ridge crest.

[57] In addition, Genovesa Ridge cones are more abundant on the ridge crest, up to 100 m taller, and more unevenly distributed than they are on the Puna Ridge [*Smith et al.*, 2002]. Many of the Puna axial cones are thought to be either rootless vents or secondary vents constructed over lava tubes supplying the large flank terraces [*Smith et al.*, 2002]. This may be the case on Genovesa Ridge as well, on the basis of the apparent connection between some of the larger segment B cones and the younger, extensive lava flow fields (F2; Figures 5 and 7). The uneven, nonlinear distribution of cone vents on Genovesa Ridge, coupled with the en echelon structure and geochemical differences imply that a single dike complex does

not underlie the entire structure, as is believed to be the case for the Puna Ridge [e.g., *Malahoff and McCoy*, 1967]. Instead, Genovesa Ridge may be supplied by a series of discontinuous dike swarms, each responsible for an individual ridge segment.

5.4. Magmatic Driving Forces and the Origins of Submarine Ridges and Platforms in the Northern Galápagos

[58] Submarine rifts on the Hawaiian volcanoes are believed to arise from lateral migration of magma from a central body, in which magmatic pressure provides the driving force for the propagation of the rift zone [e.g., *Lonsdale*, 1989]. Alternatively, ridge construction may be a passive phenomenon in which magma migrates vertically in response to extensional tectonics and fracture formation, analogous to a mid-ocean ridge system. In the former case, a single, focused magma source actively drives rift formation. In the latter, magma is drawn passively from melt pockets in the mantle immediately underlying the fractures in response to extension.

5.4.1. Active Rift Formation Model

[59] According to the current paradigm for Hawaiian volcanic rift zones, dike swarms transport magma along the ridge outward from a central body [e.g., *Pollard et al.*, 1983; *Knight and Walker*, 1988]. Such ridges are usually characterized by highly linear structures, which extend from a subaerial volcano's shoreline and possess relatively uniform slopes of a few percent (7–8%) [*Fialko and Rubin*, 1999; *Lonsdale*, 1989; *Fornari et al.*, 1978]. According to numerical and physical models, the along-axis slope is controlled primarily by laterally migrating dikes as they lose pressure with increasing distance from the magma source [*Fialko and Rubin*, 1999].

[60] One of the most striking features of the Kilauea East Rift Zone (ERZ) slopes (subaerial and submarine portions included) is the evenness of the crest over the first 100 km. There is only one major change in gradient, at the coastline, where the subaerial ERZ slope of 23 m/km steepens to 51 m/km along the Puna Ridge then continues nearly constantly to 2700 m depth [*Lonsdale*, 1989; *Smith et al.*, 2002]. This pattern is consistent with models such as those of *Lacey et al.* [1981] and *Angevine et al.* [1984] that predict magma injected at the base of a volcano will follow paths of least resistance along a surface of constant hydraulic potential, the slope of which increases below sea level. *Lonsdale* [1989] infers that the ERZ-Puna Ridge must therefore be supplied by a high, regular magma flux to maintain the equipotential surface for over 100 km along axis.

[61] Furthermore, the uniform slopes of ridges such as the Puna have been attributed to a mechanism in which the magmatic pressure from the central reservoir controls injection into the rift zone. Magma migrates along topographically controlled slopes with little or no variation in tectonic stress along strike [*Fialko and Rubin*, 1999]. Long rift zones (on the order of 100 km) must maintain relatively constant slopes for effective along-axis magma transport, because magmatic driving pressure decreases with distance from the source [*Fialko and Rubin*, 1998, 1999]. Consequently, the evenness of a ridge's slope provides a means of assessing the continuity of the intrusive dike system [e.g., *Angevine et al.*, 1984]. In shorter dike systems or those with low magmatic driving pressures, eruptions are focused near the magma source, resulting in steeper, variable axial profiles near the vent that decrease progressively with distance [*Fialko and Rubin*, 1999].

[62] The distinct en echelon structure of Genovesa Ridge is not consistent with a lateral injection model. As described above, the ridge is not a straight rift, but a sequence of at least three segments that curve toward each other at their tips. The along-axis slope of Genovesa Ridge is highly variable (Figure 6), indicating that there is not an even surface of constant hydraulic potential along the ridge controlling magma distribution. The ragged axial profile of the Genovesa Ridge suggests instead that there must be variable, localized intrusions along the rift, consistent with an irregular magma supply along strike. Consequently, magma supply to the rift is sporadic in time (irregular, limited magma flux) and/or in space (isolated dike swarms).

[63] Further support for this conclusion comes from a comparison of the axes of the Puna and Genovesa Ridges. The crest of the Puna Ridge maintains a relatively constant width across its westernmost 38 kilometers (down to 2100 m depth), varying only between 2–4 km for the majority of the segment [*Clague et al.*, 1994]. East of this point, the ridge crest becomes less well defined and considerably narrower. *Fialko and Rubin* [1998] state that a topographically driven dike should be characterized by a constant thickness along any cross-section parallel to the direction of dike propagation; this translates to a constant crestal width throughout the portion of the rift supported by the main dike complex (except near the dike nose), as is observed along the Puna Ridge. Consistently, magnetic studies of *Malahoff and McCoy* [1967] and subsequent work by *Smith et al.* [2001, 2002] confirm that virtually the entire 75-km long Puna Ridge is underlain by a dike complex ~11 km in width.

[64] In contrast, crestal widths at Genovesa Ridge vary significantly over short distances (Figures 3 and 4). The segment adjacent to Genovesa Island (A) decreases from >6.5 km at its widest point (including the almost flat island) to near zero within ~14 km; segment B pinches out completely from ~6 km at its midpoint within a mere ~9 km (Figure 3). This variability in crestal width implies discontinuous dike swarms along the axis, further ruling out a centralized, pressure-driven magma supply.

5.4.2. A Passive Extensional Rift Zone Model

[65] The structural, morphological, and geochemical characteristics of Genovesa Ridge are consistent with a passive rift zone model in which partial melts in the underlying mantle migrate in response to stresses induced by far-field tectonic forces. In an opening (mode I) crack, the local stress field at the propagating tip is complex and includes components of shear perpendicular to local maximum tensile stress. When two adjacent straight cracks overlap, the local shear component (mode II: sliding) causes the cracks to propagate out of plane, curving toward each other at increasingly sharp angles [*Lange*, 1968]. Theoretical calculations predict that interacting, en echelon fractures will have two defining characteristics: (1) as adjacent fractures approach each other, they will diverge initially before converging, taking on a hook-like path [e.g., *Pollard and Aydin*, 1984]; and (2) if propagation is driven by extensional forces, the region between the tips should experience focused extension, resulting in the formation of topographic depressions in the overlap region [*Pollard and Aydin*, 1984].

[66] Genovesa Ridge segments follow hooked paths, first diverging from each other before converging, reminiscent of overlapping spreading centers along fast spreading mid-ocean ridges (Figures 4 and 5) [e.g., *MacDonald and Fox*, 1983]. Topographic depressions exist between the segment tips, bounded by the crests of the ridge segments (Figures 4 and 5). These characteristics imply that the Genovesa Ridge segments are (1) interacting mechanically [*Olson and Pollard*, 1989]; (2) propagating from a central location; and (3) likely being formed by mode I opening caused by extensional stresses [*Thomas and Pollard*, 1993]. All of these observations are consistent with the focusing of magma by tectonic stresses as a passive response to extension.

[67] In the passive rift zone model, each segment is supplied by magma derived from the mantle immediately underlying the segment. Magma subsequently migrates toward the segment tips, resulting in the en echelon geometry. Consistently, lavas erupted from the base and crest of Genovesa Ridge appear to originate from a broad melt zone that taps the underlying depleted mantle, not necessarily from a single, interconnected magmatic system. The shallow fractionation signature (<1 kb) further precludes the existence of a long-lived magma chamber supplying the entire ridge. This process is reflected in the Genovesa Ridge morphology, including the uneven distribution of cone vents along its crest, variable crestal widths along axis, and a nonuniform axial slope, all indications that the ridge is underlain by a series of discontinuous dike swarms. The large-scale linearity of Genovesa Ridge (075°) and the western platforms (088°)

further implies that regional stress fields control the volcanic constructional process, a phenomenon predicted by the passive rift zone model.

5.5. Passive Extension in the Northern Galápagos Region

[68] The mechanism responsible for passive rifting and for the major structural trends observed in the Northern Galapagos region may be deviatoric stresses generated by interaction between the Galapagos spreading center and the hot spot [e.g., *Harpp and Geist*, 2002]. Both geochemical [e.g., *Verma and Schilling*, 1982; *Verma et al.*, 1983; *Schilling et al.*, 1982; *Detrick et al.*, 2002] and bathymetric observations [e.g., *Canales et al.*, 1997] have shown that the Galápagos hot spot and the GSC are close enough to interact extensively. The flank of a spreading center adjacent to a hot spot is weakened by thermal effects of the warm, sublithospheric plume, encouraging rifting between the plume and the ridge [*Small*, 1995]. Lithospheric cracking may be initiated along crustal weaknesses caused by large-scale tectonic stresses centered on the 91°W transform fault [e.g., *Clifton et al.*, 2000]. The tension-induced fractures could initiate passive upwelling of the underlying, depleted mantle, resulting in the observed rift zone formation.

[69] In a biaxial tensile loading model designed to reproduce the stress field around a transform fault, *Gudmundsson* [1995] proposed that extensional structures form astride the ridge when ridge-parallel tensile stress accompanies the usual ridge-perpendicular stress. The stress field generated by the model successfully reproduces the observed distribution of oblique fractures near transform faults in Iceland (Figure 11). Where ridge-perpendicular stress is dominant, fractures are parallel to the ridge; where stresses parallel to the ridge are stronger, fractures become perpendicular to the ridge. In between, fractures oblique to both the transform fault and ridge are formed when the two stresses are close to equal ($\sim$45° [*Gudmundsson*, 1995]) (Figure 11). Field studies in Iceland and on the Mid-Atlantic Ridge have noted oblique structures like those predicted by the model [e.g., *Gudmundsson*, 1995; *Gudmundsson et al.*, 1993; *Macdonald et al.*, 1986].

[70] Many of the volcanic ridges in the northern Galapagos conform to the distribution and orientation of stresses predicted around the 91°W transform fault [*Gudmundsson*, 1995]. The structural trend defining Genovesa Ridge (075°) extends through Genovesa Island to West Genovesa Ridge. Genovesa Island is crosscut by major eruptive fissures whose alignment is also parallel to the overall trend of the ridge, lending support to the regional origin of the deviatoric stresses. These fissures are tension fractures with a minor normal component and have erupted lava virtually identical to the average composition of the shield-building phases of the island [*Harpp et al.*, 2002]. The trend of the fractures shifts to nearly E-W (088°) between West Genovesa Ridge and Marchena Island, then the fractures turn northwestward toward Pinta Island.

[71] Although the trends of Genovesa Ridge and the Wolf-Darwin lineament almost exactly parallel those predicted by *Gudmundsson*'s [1995] calculations, the model does not conform to the trends of fissures and fractures directly south of the 91°W transform, near Pinta and Marchena Islands (see Figures 11b and 11c). This may be due to the boundary conditions set in the model; other calculations [e.g., *Fujita and Sleep*, 1978; *Behn et al.*, 2002] predict alternative orientations in the area beyond the transform.

[72] Theoretically, similar deviatoric stress fields should occur at all transform faults; if so, then why are volcanic provinces like the Northern Galapagos not more common at mid-ocean ridge systems? We believe the difference lies in the particular setting of the northern Galápagos, where the hot spot is located within a mere 100–200 km of the spreading center. Consequently, the mantle between the central Galapagos platform and the GSC is hotter than the average, ambient mantle near MORs that are far removed from hot spots [e.g., *Schilling*, 1991]. Whereas all transform faults likely impose regional deviatoric stresses on the surrounding lithosphere and may induce extensive networks of fractures [e.g., *Gudmundsson*, 1995; *Gudmundsson et al.*,

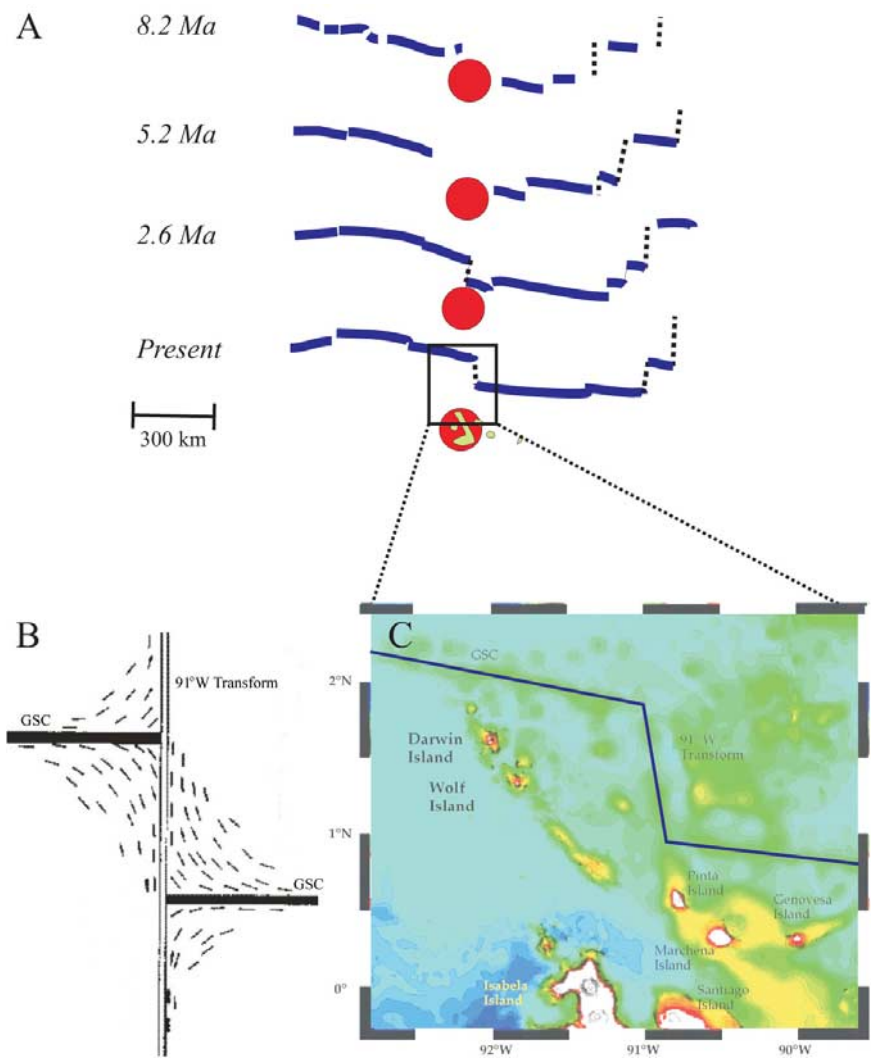

Figure 11. Conceptual model of the genesis and evolution of the Genovesa Ridge. (a) GSC-hot spot geometry over past ~8 Ma (from *Wilson and Hey* [1995]); Genovesa Ridge would have been constructed in the last <1.5 Ma. (b) Present-day regional stress field in the northern Galapagos, induced by adjacent transform fault at 91°W [*Gudmundsson*, 1995]. (c) Bathymetric map of the present-day northern Galapagos Archipelago; note broad similarity of distribution and orientation of volcanic structures to the stress field in B (see Figure 1 for reference).

1993; *Macdonald et al.*, 1986; *Clifton et al.*, 2000], it is only in the presence of high heat flow and the attendant excess magma that significant eruptive activity can occur. The serendipitous combination of the transform fault and the adjacent hot spot results in the formation of major volcanic ridges along lines of deviatoric stress, essentially illuminating the regional stress field. According to this model, Genovesa Ridge is the conjugate to the Wolf-Darwin Lineament, which has been proposed to result from tension in the inside corner of an extensional transform zone [*Harpp and Geist*, 2002].

5.6. Implications of the Passive Rift Model in the Northern Galápagos Region

[73] The model in which the Genovesa Ridge formed as the passive response to regional plume-ridge interaction implies that the entire length of the ridge, including Genovesa Island, formed penecontemporaneously. The lithosphere

underlying Genovesa Ridge is approximately 1.5 Ma [*Wilson and Hey*, 1995], placing an upper limit on its age. The lack of sediment cover on the ridges in the study area suggests that they are considerably younger than 1.5 Ma. Field studies by *Harpp et al.* [2002] indicate that Genovesa Island emerged <350 ka. Whether the island's formation marks the final stage of the entire ridge's formation or only the last step in the construction of segment A, however, requires further detailed chronological analysis unattainable with the samples in hand.

[74] According to the passive rift model, each segment of the ridges taps only the underlying mantle, with little lateral transport. Consequently, variation in depth and volume of the segments indicates that the quantity of melt available in the underlying mantle differs along the fracture set, reaching a maximum at segment A (Genovesa Island) and a minimum at segment C for Genovesa Ridge. The substantially greater volumes of Pinta and Marchena Islands (including the submarine ridges that emanate from them) further suggest that magma supply is considerably more abundant west of Genovesa Ridge. This observation is supported by the fact that lavas also become progressively more enriched westward from Genovesa, reaching a peak at Pinta Island, indicating greater contribution from the Galapagos plume [*White et al.*, 1993; *Kurz and Geist*, 1999; *Harpp et al.*, 2002]. Even though these observations are based on sparse sampling, they provide important preliminary information regarding the geographic distribution of plume material in the mantle and the dynamics of plume-ridge magmatic communication.

6. Conclusions

[75] New multibeam and side-scan sonar surveys and dredging operations indicate a volcanic origin of the Genovesa Ridge and suggest that it is recently active, probably $\ll$1.5 Ma. Clear morphologic evidence supports tectonic control of volcanism along the Genovesa Ridge, especially the aligned eruptive cones that conform to the overall ridge trend. The en echelon structure of the ridge further suggests that this feature is likely the result of extensional tectonism [*Thomas and Pollard*, 1993; *Pollard and Aydin*, 1984]. Nevertheless, the distinct lack of fractures and faults indicates that the ridge is in a largely constructional phase, in which active volcanism currently dominates over tectonic activity.

[76] Genovesa Ridge is fundamentally different in origin from Hawaiian submarine rifts. Instead of resulting from lateral propagation of dikes from a central volcano, it represents vertical ascent of magma in an environment of extensional stresses near a plate boundary. Geochemical evidence indicates that the Genovesa Ridge lavas are derived from depleted mantle sources similar to those of Genovesa Island and experienced shallow fractionation and mixing with magmas of variable temperatures prior to eruption. These observations suggest that Genovesa Ridge lavas may be supplied from a broad melt zone directly underlying the ridge.

[77] Genovesa Ridge and its western extensions appear to be the result of passive upwelling directed by far-field tectonic stresses generated by tension across the 91°W transform [e.g., *Gudmundsson*, 1995; *Harpp and Geist*, 2002]. The proximity of the plume causes magmatism in the extensional zones where it would not ordinarily occur. Limited coverage of the seafloor west of Genovesa Island implies that similar elongate structures that extend toward Pinta Island may also have formed in a related process.

Acknowledgments

[78] The authors would like to thank the Captain and crew of the R/V Revelle, Gene Pillard the Res. Tech., Uta Peckman for multibeam data processing, and Daniel Jacobson for shipboard computer support, as well as the scientific party of the DRIFT04 cruise leg. We would also like to extend our gratitude to the Government of Ecuador, the Galapagos National Park, and the staff of the Charles Darwin Research Station for their support of our project. Special thanks go to Roger Goldsmith and Paul Johnson for assistance with figure production. Thanks to Art Goldstein for helpful discussions early in the paper's evolution. This work has been generously supported by the National Science Foundation, Ocean Sciences Division, Marine Geology and Geophysics grant OCE-0002461 (to Kurz, Fornari, and Geist), CHE-9996141 and CHE-9996136 (to Harpp), EAR-0126097 (to Kurz), OCE-0002818 and EAR-0002818 (to Geist).

References

Angevine, C. L., D. L. Turcotte, and J. R. Ockendon, Geometrical form of aseismic ridges, volcanoes, and seamounts, *J. Geophys. Res.*, *89*, 11,287–11,292, 1984.

Behn, M. D., J. Lin, and M. T. Zuber, Evidence for weak oceanic transform faults, *Geophys. Res. Lett.*, *29*, 2207, 2002.

Canales, J. P., J. J. Danobeitia, R. S. Detrick, E. E. E. Hooft, R. Bartolome, and D. R. Naar, Variations in axial morphology along the Galápagos Spreading Center and the influence of the Galápagos hotspot, *J. Geophys. Res.*, *102*, 27,341–27,354, 1997.

Chadwick, W. W., and K. A. Howard, The pattern of circumferential and radial eruptive fissures on the volcanoes of Fernandina and Isabela islands, Galápagos, *Bull. Volcanol.*, *53*, 259–275, 1991.

Christie, D. M., and C. Fox, Morphologic evolution of the margins of the Galápagos Platform, *Eos Trans. AGU*, *71*(43), 1578, 1990.

Clague, D. A., et al., Bathymetry of Puna Ridge, Kilauea Volcano, Hawaii, *U.S., Geol. Surv. Misc. Field Stud. Map, MF-2237*, 1994.

Clague, D. A., J. G. Moore, J. E. Dixon, and W. B. Friesen, Petrology of submarine lavas from Kilauea's Puna Ridge, *Hawaii, J. Petrol.*, *36*, 299–349, 1995.

Clague, D. A., J. G. Moore, and J. R. Reynolds, Formation of submarine flat-topped volcanic cones in Hawaii, *Bull. Volcanol.*, *62*(3), 214–233, 2000.

Clifton, A. E., R. W. Schlische, M. O. Withjack, and R. V. Ackermann, Influence of rift obliquity on fault-population systematics: Results of experimental clay models, *J. Struct. Geol.*, *22*, 1491–1509, 2000.

Cullen, A. B., and A. R. McBirney, The volcanic geology and petrology of Isla Pinta, Galapagos archipelago, *Bull. Geol. Soc. Am.*, *98*, 294–301, 1987.

Cullen, A. B., E. Vicenzi, and A. R. McBirney, Plagioclase-ultraphyric basalts of the Galápagos Archipelago, *J. Volcanol. Geotherm. Res.*, *37*, 325–337, 1989.

Davis, R., S. Zisk, M. Simpson, M. Edwards, A. Shor, and E. Halter, Hawaii Mapping Research Group bathymetric and sidescan data processing, in *Oceans '93: Engineering in Harmony With the Ocean: Proceedings*, vol. II, pp. 449–453, IEEE Press, Piscataway, N. J., 1993.

DeMets, C., R. G. Gordon, D. R. Argus, and S. Stein, Effect of recent revisions to the geomagnetic reversal time scale on estimate of current plate motions, *Geophys. Res. Lett.*, *21*, 2191–2194, 1994.

Detrick, R. S., J. M. Sinton, G. Ito, J. P. Canales, M. Behn, T. Blacic, B. Cushman, J. E. Dixon, D. W. Graham, and J. J. Mahoney, Correlated geophysical, geochemical, and volcanological manifestations of plume-ridge interaction along the Galápagos Spreading Center, *Geochem. Geophys. Geosyst.*, *3*(10), 8501, doi:10.1029/2002GC000350, 2002.

Eggins, S. M., et al., A simple method for the precise determination of > or = 40 trace elements in geological samples by ICPMS using enriched isotope internal standardisation, *Chem. Geol.*, *134*(4), 311–326, 1997.

Fialko, Y. A., and A. M. Rubin, Thermodynamics of lateral dike propagation; implications for crustal accretion at slow spreading mid-ocean ridges, *J. Geophys. Res.*, *103*, 2501–2514, 1998.

Fialko, Y. A., and A. M. Rubin, What controls the along-strike slopes of volcanic rift zones?, *J. Geophys. Res.*, *104*, 20,007–20,021, 1999.

Fornari, D. J., et al., Axial summit trough of the East Pacific Rise 9°–10°N: Geological characteristics and evolution of the axial zone on fast spreading mid-ocean ridges, *J. Geophys. Res.*, *103*, 9827–9855, 1998.

Fornari, D. J., A. Malahoff, and B. C. Heezen, Volcanic structure of the crest of the Puna Ridge, Hawaii: Geophysical implications of submarine volcanic terrain, *Geol. Soc. Am. Bull.*, *89*(4), 605–616, 1978.

Fornari, D. J., M. D. Kurz, D. J. Geist, P. D. Johnson, U. G. Peckman, and D. Scheirer, New perspectives on the structure and morphology of the submarine flanks of Galápagos volcanoes—Fernandina and Isabela, *Eos Trans. AGU*, *82*(47), Fall Meet. Suppl., Abstract T41D-06, 2001.

Fujita, K., and N. Sleep, Membrane stresses near mid-ocean ridge-transform intersections, *Tectonophysics*, *50*, 207–221, 1978.

Geist, D. J., W. M. White, and A. R. McBirney, Plume-asthenosphere mixing beneath the Galápagos Archipelago, *Nature*, *333*, 657–660, 1988.

Geist, D. J., T. R. Naumann, and P. L. Larson, Evolution of Galápagos magmas: Mantle and crustal fractionation without assimilation, *J. Petrol.*, *39*, 953–971, 1998.

Ghiorso, M. S., and R. O. Sack, Chemical mass transfer in magmatic processes; IV, A revised and internally consistent thermodynamic model for the interpolation and extrapolation of liquid-solid equilibria in magmatic systems at elevated temperatures and pressures, *Contrib. Mineral. Petrol.*, *119*(2–3), 197–212, 1995.

Graham, D. W., D. M. Christie, K. S. Harpp, and J. E. Lupton, Mantle plume helium in submarine basalts from the Galápagos platform, *Science*, *262*, 2023–2026, 1993.

Gripp, A. E., and R. G. Gordon, Current plate velocities relative to the hotspots incorporating the NUVEL-1 global plate motion model, *Geophys. Res. Lett.*, *17*, 1109–1112, 1990.

Gripp, A. E., and R. G. Gordon, Young tracks of hotspots and current plate velocities, *Geophys. J. Int.*, *150*(2), 321–361, 2002.

Gudmundsson, A., Stress fields associated with oceanic transform faults, *Earth Planet. Sci. Lett.*, *136*, 603–614, 1995.

Gudmundsson, A., S. Brynjolfsson, and M. T. Jonsson, Structural analysis of a transform fault-rift zone junction in north Iceland, *Tectonophysics*, *220*(1–4), 205–221, 1993.

Harpp, K. S., and D. J. Geist, Wolf-Darwin lineament and plume–ridge interaction in northern Galápagos, *Geochem. Geophys. Geosyst.*, *3*(11), 8504, doi:10.1029/2002GC000370, 2002.

Harpp, K. S., and W. M. White, Tracing a mantle plume: Isotopic and trace element variations of Galápagos seamounts, *Geochem. Geophys. Geosyst.*, *2*(6), Paper number 2000GC000137, 2001.

Harpp, K. S., K. R. Wirth, and D. J. Korich, Northern Galápagos Province: Hotspot-induced, near-ridge volcanism at Genovesa Island, *Geology*, *30*, 399–402, 2002.

Holcomb, R. T., Eruptive history and long-term behavior of Kilauea volcano, *U.S. Geol. Surv. Prof. Pap.*, *1350*, 261–350, 1987.

Holcomb, R. T., J. G. Moore, P. W. Lipman, and R. H. Belderson, Voluminous submarine lava flows from Hawaiian volcanoes, *Geology*, *16*, 400–404, 1988.

Johnson, D. M., P. R. Hooper, and R. M. Conrey, XRF analysis of rocks and minerals or major and trace elements on a single low dilution Li-tetraborate fused bead, *Adv. X Ray Anal.*, *41*, 843–867, 1999.

Johnson, K. T. M., J. R. Reynolds, D. Vonderhaar, D. K. Smith, and L. S. L. Kong, Petrological systematics of submarine basalt glasses from the Puna Ridge, Hawaii: Implications for rift zone plumbing and magmatic processes, in *Hawaiian Volcanoes: Deep Underwater Perspectives*, *Geophys. Monogr. Ser.*, vol. 128, edited by E. Takahashi et al., 143–161, AGU, Washington, D. C., 2002.

Knight, M. D., and G. P. L. Walker, Magma flow directions in dikes of the Koolau Complex, Oahu, determined from magnetic fabric studies, *J. Geophys. Res.*, *93*, 4301–4319, 1988.

Kurz, M. D., and D. Geist, Dynamics of the Galápagos hotspot from helium isotope geochemistry, *Geochim. Cosmochim. Acta*, *63*, 4139–4156, 1999.

Kurz, M. D., T. Kenna, D. Kammer, J. M. Rhodes, and M. O. Garcia, Isotopic evolution of Mauna Loa volcano: A view from the submarine south west rift, in *Mauna Loa Revealed: Structure, Composition, History and Hazards*, *Geophys. Monogr. Ser.*, vol. 92, edited by J. P. Lockwood and J. M. Rhodes, pp. 289–306, AGU, Washington, D. C., 1995.

Kurz, M. D., D. J. Fornari, D. Geist, P. Johnson, J. Curtice, D. Lott, K. Harpp, A. Saal, and U. Peckman, The leading edge of the Galapagos hotspot: Geochemistry and geochronology of submarine glasses coupled to new sidescan sonar imagery, *Eos Trans. AGU*, *82*(47), Fall Meet. Suppl., Abstract T42B-0938, 2001.

Lacey, A., J. R. Ockendon, and D. L. Turcotte, On the geometrical form of volcanoes, *Earth Planet. Sci. Lett.*, *54*(1), 139–143, 1981.

Lange, F. F., Interaction between overlapping parallel cracks: A photoelastic study, *Int. J. Fract. Mech.*, *4*, 287–294, 1968.

Lipman, P. W., W. R. Normark, J. G. Moore, J. B. Wilson, and C. E. Gutmacher, The giant submarine Alika debris slide, Mauna Loa, Hawaii, *J. Geophys. Res.*, *93*, 4279–4299, 1988.

Lipman, P. W., T. W. Sisson, T. Ui, and J. Naka, In search of ancestral Kilauea Volcano, *Geology*, *28*, 1079–1982, 2000.

Lonsdale, P., A geomorphological reconnaissance of the submarine part of the East Rift Zone of Kilauea Volcano, Hawaii, *Bull. Volcanol.*, *51*, 123–144, 1989.

Macdonald, K. C., and P. J. Fox, Overlapping spreading centres; new accretion geometry on the East Pacific Rise, *Nature*, *302*, 55–58, 1983.

Macdonald, K. C., et al., Deep-tow studies of the Vema fracture zone: 1. Tectonics of a major slow slipping transform fault and its intersection with the Mid-Atlantic Ridge, *J. Geophys. Res.*, *91*, 3334–3354, 1986.

Malahoff, A., and F. McCoy, The geologic structure of the Puna submarine ridge, Hawaii, *J. Geophys. Res.*, *72*(2), 541–548, 1967.

McDonough, W. F., and S. S. Sun, The composition of the Earth, *Chem. Geol.*, *120*, 223–253, 1995.

Moore, J. G., and R. S. Fiske, Volcanic substructure inferred from dredge samples and ocean-bottom photographs, Hawaii, *Geol. Soc. Am. Bull.*, *80*(7), 1191–1201, 1969.

Olson, J., and D. D. Pollard, Inferring paleostresses from natural fracture patterns; a new method, *Geology*, *17*(4), 345–348, 1989.

Plank, T., and C. H. Langmuir, Effects of the melting regime on the composition of the oceanic crust, *J. Geophys. Res.*, *97*, 19,749–19,770, 1992.

Pollard, D. D., and A. Aydin, Propagation and linkage of oceanic ridge segments, *J. Geophys. Res.*, *89*, 10,017–10,028, 1984.

Pollard, D. D., et al., Surface deformation in volcanic rift zones, *Tectonophysics*, *94*, 541–584, 1983.

Rongstadt, M., HAWAII MR-1: A new underwater mapping tool, paper presented at International Conference on Signal Processing and Technology, Inst. of Electr. and Electron, Eng., San Diego, Calif., 1992.

Schilling, J.-G., Fluxes and excess temperatures of mantle plumes inferred from their interaction with migrating mid-ocean ridges, *Nature*, *352*, 397–403, 1991.

Schilling, J.-G., R. H. Kingsley, and J. D. Devine, Galapagos hot spot-spreading center system: 1. Spatial, petrological, and geochemical variations (83°W–101°W), *J. Geophys. Res.*, *87*, 5593–5610, 1982.

Sinton, J. M., and R. Detrick, Mid-ocean ridge magma chambers, *J. Geophys. Res.*, *97*, 197–216, 1992.

Slater, L., D. McKenzie, K. Grönvold, and N. Shimizu, Melt generation and movement beneath Theistareykir, NE Iceland, *J. Petrol.*, *42*, 321–354, 2001.

Small, C., Observations of ridge-hotspot interactions in the Southern Ocean, *J. Geophys. Res.*, *100*, 17,931–17,946, 1995.

Smith, D. K., and J. R. Cann, Constructing the upper crust of the Mid-Atlantic Ridge: A reinterpretation based on the Puna Ridge, Kilauea Volcano, *J. Geophys. Res.*, *104*, 25,379–25,399, 1999.

Smith, D. K., and T. H. Jordan, Seamount statistics in the Pacific Ocean, *J. Geophys. Res.*, *93*, 2899–2918, 1988.

Smith, D. K., M. A. Tivey, P. M. Gregg, and L. S. L. Kong, Magnetic anomalies at the Puna Ridge, a submarine extension of Kilauea Volcano: Implications for lava deposition, *J. Geophys. Res.*, *106*, 16,047–16,060, 2001.

Smith, D. K., L. S. L. Kong, K. T. M. Johnson, and J. R. Reynolds, Volcanic morphology of the submarine Puna Ridge, Kilauea Volcano, in *Hawaiian Volcanoes: Deep Underwater Perspectives*, edited by E. Takahashi et al., *Geophys. Monogr. Ser.*, vol. 128, pp. 125–142, Washington, D. C., 2002.

Smith, W. H. F., and D. T. Sandwell, Global sea floor topography from satellite altimetry and ship depth soundings, *Science*, *277*, 1956–1962, 1997.

Thomas, A. L., and D. D. Pollard, The geometry of echelon fractures in rock; implications from laboratory and numerical experiments, *J. Struct. Geol.*, *15*(3–5), 323–334, 1993.

Toomey, D. R., E. E. E. Hooft, S. Solomon, D. James, and M. Hall, Upper mantle structure beneath the Galápagos Archipelago from body wave data, *Eos Trans. AGU*, *82*(47), Abstract T41D-04, 2001.

Verma, S. P., and J.-G. Schilling, Galapagos hot spot-spreading center system: 2. $^{87}Sr/^{86}Sr$ and large ion lithophile element variations (85°W–101°W), *J. Geophys. Res.*, *87*, 10,838–10,856, 1982.

Verma, S. P., J.-G. Schilling, and D. G. Waggoner, Neodymium isotopic evidence for Galápagos hotspot-spreading center system evolution, *Nature*, *306*, 654–657, 1983.

White, W. M., A. R. McBirney, and R. A. Duncan, Petrology and geochemistry of the Galápagos Islands: Portrait of a pathological mantle plume, *J. Geophys. Res.*, *98*, 19,533–19,564, 1993.

Wilson, D. S., Focused mantle upwelling beneath mid-ocean ridges; Evidence from seamount formation and isostatic compensation of topography, *Earth Planet. Sci. Lett.*, *113*, 41–55, 1992.

Wilson, D. S., and R. N. Hey, History of rift propagation and magnetization intensity for the Cocos-Nazca spreading center, *J. Geophys. Res.*, *100*, 10,041–10,056, 1995.